Electronic Supplementary Material (ESI) for Inorganic Chemistry Frontiers.

Supporting Information

Designing Structurally Tunable and Functionally Versatile Synthetic Supercontainers

Feng-Rong Dai, [a,b] *Yupu Qiao,* [b] *and Zhenqiang Wang* [b]*

a) State Key Laboratory of Structural Chemistry, Fujian Institute of Research on the Structure of Matter, Chinese Academy of Sciences, Fuzhou, Fujian 350002, China

b) Department of Chemistry, The University of South Dakota, Churchill-Haines Laboratories, Room 115, 414 East Clark Street, Vermillion, South Dakota 57069-2390, United States

* To whom correspondence should be addressed. E-mail: Zhenqiang.Wang@usd.edu. Telephone: (605) 677-7281. Fax: (605) 677-6397.

General Methods

Unless otherwise noted, starting materials and solvents were obtained from commercial suppliers (Fisher Scientific, TCI, Alfa Aesar, Cambridge Isotope Laboratories, Inc., etc.; **H_2L1** was purchased from Matrix Scientific) and used without further purification. *p-tert*-Butylsulfonylcalix[4]arene (TBSC) [S1, S2] was synthesized as described in the literature.

^{1}H and ^{13}C NMR spectra were measured on a Bruker 400 MHz NMR instrument (400 MHz for ^{1}H NMR and 100 MHz for ^{13}C NMR). Tetramethylsilane (TMS) was used as the internal standard for ^{1}H NMR, and $CDCl_3$ served as the internal standard for ^{13}C NMR. The following abbreviations were used to express the multiplicities: s = singlet; d = doublet; t = triplet; q = quartet; m = multiplet; br = broad.

UV-vis studies were done on a Varian Cary 5000 UV-Vis-NIR spectrophotometer at room temperature. Mass spectra were collected on a Varian 500-MS Ion Trap Mass Spectrometer using an ESI negative mode. Thermogravimetric analysis (TGA) was performed at a scan speed of 2 °C/min under a stream of nitrogen on a TA Instruments Q600 SDT. Typical sample size for TGA experiments was ~5-10 mg. A CE-440 elemental analyzer (EAI Exeter Analytical Inc., North Chelmsford, Massachusetts) was used to determine the weight fraction of carbon, hydrogen and nitrogen. Elemental analysis results were based on the average of two or more trials for each sample.

Gas adsorption isotherms were measured using a Micromeritics ASAP2020 instrument based on a volumetric method. Samples were typically washed with methanol and pre-dried on a Schlenk line at 120 °C for 8 h before transferred to pre-weighed analysis tubes which were then capped with seal frits. The samples were degassed under dynamic vacuum (< 6 μmHg) at 105 °C for ~24-48 h until the outgas rates were lower than 5 μmHg/min. The analysis tubes containing the evacuated samples were weighed again to determine the sample weights (typically ~100 mg for most samples) before transferred back to the analysis port of the instrument. The H_2, N_2 and O_2 isotherms were measured at 77 K in a liquid N_2

bath using ultra high pure (UHP) grade gases (99.99%), the CO_2 isotherms were measured at 196 K in a dry ice/isopropanol bath using ultra high pure (UHP) grade CO_2 gas (99.99%).

Synthesis

H_2L2: The ligand **H_2L2** was synthesized according to the reported method. [S3] 4-Carboxybenzaldehyde (1.50 g, 10 mmol) in MeOH (50 ml) was added to a MeOH solution (50 ml) of 4-aminobenzoic acid (1.37 g, 10 mmol) with stirring, upon which a yellow solid formed immediately. The mixture was stirred for 2 h. The intermediate Schiff base that formed was then reduced with an excess of $NaBH_4$. Briefly, to the aforementioned mixture was added 1.00 g. (26.00 mmol) of $NaBH_4$ in small portions over 5 minutes and the resulting mixture was stirred for an additional 30 minutes. The insoluble residue was filtered off and the filtrate was dried by rotary evaporation. The residue was then dissolved in 100 mL water and the pH of the aqueous solution was adjusted to 5.0 using HCl solution (1.0 mol L^{-1}). The off-white solid was filtered off, washed with Et_2O, dried, and recrystallized from MeOH/H_2O (3:1). Yield: 1.90 g, 70%. ^{1}H NMR (400 MHz, $CDCl_3$): δ = 12.48 (s, 2H), 7.90 (d, *J* = 8.28 Hz, 2H, Ar-H), 7.64 (d, *J* = 8.72 Hz, 2H, Ar-H), 7.45 (d, *J* = 8.28 Hz, 2H, Ar-H), 7.12 (t, *J* = 6.12 Hz, 1H, -NH-), 6.58 (d, *J* = 8.80 Hz, 2H, Ar-H), 4.42 (d, *J* = 6.08 Hz, 2H, -CH_2-) ppm.

H_2L3: The preparation of **H_2L3** was similar to that of **H_2L2** except that 4-(aminomethyl)benzoic acid (1.51 g, 10 mmol) was used in place of 4-aminobenzoic acid. Yield: 1.72 g, 60%. ^{1}H NMR (400 MHz, $CDCl_3$): δ = 7.92 (d, *J* = 7.28 Hz, 4H, Ar-H), 7.53 (d, *J* = 6.84 Hz, 4H, Ar-H), 3.92 (s, 4H, -CH_2-) ppm.

1-Co: $Co(NO_3)_2 \cdot 6H_2O$ (145.5 mg, 0.50 mmol), **H_2L1** (56.4 mg, 0.22 mmol) and TBSC (84.9 mg, 0.10 mmol) were dissolved in 12 mL of *N*,*N*-dimethylformamide (DMF). The solution was then divided into equal portions in ten 4-mL dram vials. The vials were placed in a sand bath, which was transferred to a programmable oven and heated at a rate of 0.5 °C/min from 35 to 100 °C. The temperature was held at 100 °C for 24 h before the oven was cooled at a rate of 0.2 °C/min to a final temperature of 35 °C. Pink

crystals of **1-Co** were isolated by washing with methanol and dried in the air to give 50.2 mg of the as-synthesized material.

2-Co: $Co(NO_3)_2 \cdot 6H_2O$ (145.5 mg, 0.50 mmol), **H_2L2** (89.5 mg, 0.33 mmol) and TBSC (84.9 mg, 0.10 mmol) were dissolved in a mixture solvent of DMF (20 mL) and MeOH (10 mL). The solution was then divided into equal portions in ten 4-mL dram vials. The vials were placed in a sand bath, which was transferred to a programmable oven and heated at a rate of 0.5 °C/min from 35 to 100 °C. The temperature was held at 100 °C for 24 h before the oven was cooled at a rate of 0.2 °C/min to a final temperature of 35 °C. Pink crystals of **2-Co** were isolated by washing with methanol and dried in the air to give 58.4 mg of the as-synthesized material.

3-Ni: $Ni(NO_3)_2 \cdot 6H_2O$ (145.5 mg, 0.50 mmol), **H_2L3** (89.5 mg, 0.33 mmol) and TBSC (84.9 mg, 0.10 mmol) were dissolved in a mixture solvent of DMF (12 mL) and MeOH (6 mL). The solution was then divided into equal portions in ten 4-mL dram vials. The vials were placed in a sand bath, which was transferred to a programmable oven and heated at a rate of 0.5 °C/min from 35 to 100 °C. The temperature was held at 100 °C for 24 h before the oven was cooled at a rate of 0.2 °C/min to a final temperature of 35 °C. Green crystals of **3-Ni** were isolated by washing with methanol and dried in the air to give 84.8 mg of the as-synthesized material.

X-Ray Crystallography. X-ray single-crystal diffraction data were collected at 100 K using graphite-monochromated Mo-Kα radiation (λ = 0.71073 Å) on a Bruker CCD APEXII diffractometer. The collected frames were processed with the software SAINT. [S4] The data were corrected for absorption using the SADABS program. [S5] The structure was solved by the Direct methods (SHELX97) [S6] in conjunction with standard difference Fourier techniques and subsequently refined by full-matrix least-squares analyses on F^2. Hydrogen atoms were generated in their idealized positions and all non-hydrogen atoms were refined anisotropically. The electron count due to disordering solvents in the void space of the crystals of compounds **2-Co** and **3-Ni** was calculated using the program SQUEEZE in

PLATON software package. [S7] CCDC 1422947-1422949 contain the supplementary crystallographic data for this paper. These data can be obtained free of charge from the Cambridge Crystallographic Data Centre via www.ccdc.cam.ac.uk/data_request/cif.

Liquid-Liquid Extraction. Aqueous stock solutions of methylene blue (MB), eosin Y (EY) and methyl orange (MO) were prepared by dissolving the dye in deionized water. Different concentrations of dye solutions were prepared by step-by-step dilution of the stock solution with deionized water. 5 mL of the aqueous dye solution (2×10^{-5} ~ 6×10^{-5} M) was then added to 5 ml of chloroform solution containing the MOSC (4×10^{-6} ~ 1.2×10^{-5} M). The mixture was shaken for 1 min and kept in dark at room temperature for 4 h prior to UV-vis measurements, allowing the aqueous and chloroform layers to fully separate. Control experiments were set up in a similar manner except the MOSC solutions were replaced by straight chloroform solvents. The UV-vis spectra of the aqueous and chloroform phases were recorded on a spectrophotometer. The remaining concentration of MB in the aqueous phase was directly determined on the basis of the absorbance at 664 nm, using previously determined calibration curve. The concentration of MB in the chloroform phase was calculated by subtracting the remaining dye concentration in the aqueous solution from the dye concentration of the aqueous stock solution.

Dye Separation. Aqueous stock solutions of MB, EY and MO were prepared by dissolving the dye in deionized water. The mixed dyes solution of MB-EY and MB-MO were prepare by mixing the MB with EY and MO, respectively, in a mole ratio of 1:1, and then further diluted to a concentration of ~1×10^{-5} M. 5 mL of the aqueous dye mixture solution was then added onto 5 ml of chloroform solution containing the MOSC (~5×10^{-6} M). The mixture was shaken for 1 min and kept in dark at room temperature for 4h prior to UV-vis measurements, allowing the aqueous and chloroform layers to fully separate. Control experiments were set up in a similar manner except the MOSC solutions were replaced by straight chloroform solvent. The UV-vis spectra of the aqueous and chloroform phases were recorded on a spectrophotometer.

Homogeneous-Solution Guest Binding. The solution host-guest chemistry was probed using the UV-vis titration technique. [S8] Stock solutions of the MOSCs in $CHCl_3$ were prepared at a concentration of ~5×10^{-6} M. 25.00 mL of the stock solution was then used to dissolve an accurately known mass of MB, chosen to yield a solution at a concentration 20~100 times that of the MOSC solution. 2.00 ml of the MOSC solution was placed in a 10.0-mm quartz cell, upon which increasing portions of the MB solution were gradually added (10-μL per portion; the total volume added was 2.00 mL). After each addition, the cell was stoppered and inverted to ensure complete mixing of the solution, and the UV-vis spectrum was collected (at 25°C) after 5 minutes to ensure that the equilibrium was reached.

In order to evaluate the overall binding strength, the titration results were fitted to the linear form of Benesi-Hildebrand (B-H) equation [S9]:

$$\frac{1}{\Delta A} = \frac{1}{l\Delta\varepsilon[G]_0[H]_0K_a} + \frac{1}{l\Delta\varepsilon[H]_0}$$

where ΔA (= A_{obs} - A_0) is the change in absorbance, l (= 1 cm) is the path length, $\Delta\varepsilon$ (= $\varepsilon^{HG} - \varepsilon^{H}$) is the difference in extinction coefficient between host-guest complex and free MOSC, $[G]_0$ is initial guest concentration, $[H]_0$ is initial MOSC concentration, and K_a is the association constant.

Rhodamine B isomerization. Rhodamine B isomerization experiments were monitored by the UV-vis titration technique. Stock solutions of Rhodamine B Base (RBB) in $CHCl_3$ were prepared at a concentration of ~5×10^{-6} M. 25.00 mL of the RBB stock solution was then used to dissolve an accurately known mass of type IV MOSCs or TBSC, chosen to yield a solution at a concentration 20~100 times that of the RBB solution. 2.00 ml of the RBB solution was placed in a 10.0-mm quartz cell, upon which increasing portions of the MOSC or TBSC solution, or straight $CHCl_3$ were gradually added (10-μL per portion; the total volume added was 2.00 mL). After each addition, the cell was stoppered and inverted to ensure complete mixing of the solution, and the UV-vis spectrum was collected (at 25°C) after 5 minutes to ensure that the equilibrium was reached. To calculate the fraction conversions of RBB to RB, we

performed a reference experiment in which the same RBB solution was treated with an excess amount of a strong base Et_3N, which led to complete conversion of the RBB form to the RB form. The fraction conversion of RBB for each titration was thus obtained by determining the ratio of the UV-vis absorption intensity (at 550 nm) of the titrated solution to that of the reference solution.

The MB-exchange experiments were carried out in a similar manner. Stock solutions of RBB in $CHCl_3$ charged with type IV MOSC or TBSC (in a molar ratio of 3:1) were prepared at a concentration of ~5×10^{-6} M. 25.00 mL of the stock solution was then used to dissolve an accurately known mass of MB, chosen to yield a solution at a concentration 20~100 times that of the RBB solution. Increasing portions of the MB solution were then gradually added to the RBB-MOSC or RBB-TBSC mixture and the solution was monitored by the UV-vis technique.

Knoevenagel Condensation. Prior to the catalytic reactions, the MOSC samples were typically pre-treated with heating under vacuum at 160ºC for 8 h and TBSC at 100ºC for 5 h. A 4-mL screw-top vial was charged with 2-naphthaldehyde (62.5 mg, 0.400 mmol), malononitrile (26.4 mg, 0.400 mmol), $CHCl_3$ (4 mL) and a stirring bar. Except for the control experiment where no catalyst was used, 1 mol% of a type IV MOSC, 2 mol% of TBSC, or 4 mol% of **Me_2L3** (**L3** methyl diester), was also added to the mixture. The vial was then capped and stirred at room temperature for 48 h. The reaction product was purified by flash chromatography (hexanes: ethyl acetate, 8:1 v/v) to afford the pure product. ^{1}H NMR (400 MHz, $CDCl_3$): δ = 8.24 (d, *J* = 0.8 Hz, 1H), 8.05 (dd, *J* = 2, 8.8 Hz, 1H), 7.84 (m, 2H), 7.88 (m, 2H), 7.69 (dt, *J* =1.2, 8.0 Hz, 1H), 7.62 (dt, *J* =1.2, 8.0 Hz, 1H) ppm; ^{13}C NMR (100 MHz, $CDCl_3$) δ = 159.6, 135.7, 134.4, 132.5, 129.9, 129.6, 129.5, 128.4, 127.9, 127.7, 124.1, 113.9, 112.8, 82.1 ppm; The spectroscopic data are consistent with a previous report.[S10]

Table S1. Crystallographic Data for Compounds **1-Co**, **2-Co**, and **3-Ni**.

	1-Co	**2-Co**	**3-Ni**
Empirical formula	$C_{164}H_{188}Co_8N_8O_{50}S_8$	$C_{140}H_{136}Co_8N_4O_{42}S_8$	$C_{144}H_{144}N_4Ni_8O_{42}S_8$
Formula weight	3799.14	3274.45	3328.79
Temperature (K)	100(2)	100(2)	100(2)
Crystal system	Triclinic	Tetragonal	Triclinic
space group	$P\bar{1}$	*P*4/mnc	$P\bar{1}$
a (Å)	12.9710(6)	17.1548(12)	12.968(2)
b (Å)	13.7364(6)	17.1548(12)	13.910(3)
c (Å)	26.0130(11)	37.599(3)	27.919(5)
α (°)	79.687(1)	90	79.284(2)
β (°)	81.655(1)	90	83.244(2)
γ (°)	67.106(1)	90	67.342(2)
V (Å^3)	4186.2(3)	11065.0(13)	4560.6(15)
Z	1	2	1
D(calcd) (g cm^{-3})	1.507	0.983	1.212
μ (Mo K_α) (mm^{-1})	0.958	0.713	0.965
F(000)	1972	3368	1724
θ range (°)	1.87 - 25.00	1.08 - 20.65	0.74 - 22.81
Limiting indices	-15≤h≤15	-16≤h≤17	-14≤h≤14
	-16≤k≤16	-17≤k≤16	-15≤k≤15
	-30≤l≤30	-37≤l≤37	-30≤l≤30
Reflections collected / unique	41176 / 14679	67562 / 2892	35816 / 12326
	[R_{int} = 0.0224]	[R_{int} = 0.0811]	[R_{int} = 0.0419]
Data / restraints / parameters	14679 / 85 / 1100	2892 / 24 / 241	12326 / 12 / 940
GOF	1.056	1.088	1.078
R_1 (I>2σ(I))	0.0803	0.0828	0.0487
wR_2 (I>2σ(I))	0.2101	0.2373	0.1341
R_1 (all data)	0.0927	0.1136	0.0631
wR_2 (all data)	0.2233	0.2622	0.1410
Δρ / e A$^{\circ-3}$	4.358, -1.316	0.979, -0.421	1.303, -0.414

Table S2. Elemental analysis results for **1-Co**, **2-Co** and **3-Ni**.

Compound	Formula	Calculated			Experimental		
		C%	H%	N%	C%	H%	N%
	$[C_{140}H_{132}Co_8O_{42}S_8]$	52.31	4.14	0			
1-Co	$[C_{140}H_{132}Co_8O_{42}S_8]\cdot(DMF)_3$	52.12	4.49	1.22	48.69±0.56	4.43±0.12	1.35±0.02
	$[C_{140}H_{132}Co_8O_{42}S_8]\cdot(DMF)_4$	52.06	4.60	1.60			
	$[C_{140}H_{136}Co_8N_4O_{42}S_8]$	51.35	4.19	1.71			
2-Co	$[C_{140}H_{136}Co_8N_4O_{42}S_8]\cdot(DMF)_2$	51.26	4.42	2.46	49.65±0.01	4.62±0.01	2.52±0.01
	$[C_{140}H_{136}Co_8N_4O_{42}S_8]\cdot(DMF)_3$	51.22	4.53	2.81			
	$[C_{144}H_{144}Ni_8N_4O_{42}S_8]$	51.96	4.36	1.68			
3-Ni	$[C_{144}H_{144}Ni_8N_4O_{42}S_8]\cdot(DMF)_2$	51.85	4.58	2.42	47.76±0.01	4.62±0.06	2.31±0.04
	$[C_{144}H_{144}Ni_8N_4O_{42}S_8]\cdot(DMF)_3$	51.79	4.69	2.76			

Table S3. Comparison of experimental and calculated exact mass data of **1-Co**, **2-Co** and **3-Ni**.

Compound	Fragment	Calculated	Experimental
1-Co	$[M+5H_2O-L1-2H]^{2-}$ $C_{125}H_{128}Co_8O_{43}S_8^{2-}$	1523.0	1521.1
	$[M-2H]^{2-}$ $C_{140}H_{130}Co_8O_{42}S_8^{2-}$	1606.0	1605.9
2-Co	$[M-2H]^{2-}$ $C_{140}H_{134}Co_8N_4O_{42}S_8^{2-}$	1636.0	1636.5
3-Ni	$[M+2CH_3CN-L3-2H]^{2-}$ $C_{132}H_{133}N_5Ni_8O_{38}S_8^{2-}$	1560.6	1561.4
	$[M+H_2O-2H]^{2-}$ $C_{144}H_{144}N_4Ni_8O_{43}S_8^{2-}$	1671.0	1670.2

Table S4. Concentrations ($\times 10^{-6}$ mol/L) of Type IV MOSCs in chloroform, and of MB in aqueous phase before ($[MB]_{0,\,aq}$) and after ($[MB]_{1,\,aq}$) extraction experiments.

	1-Co				2-Co			
Entry	$[MB]_{0,\,aq}$	$[MB]_{1,\,aq}$	[MOSC]	**[MB]/[MOSC]**	$[MB]_{0,aq}$	$[MB]_{1,aq}$	[MOSC]	**[MB]/[MOSC]**
1	96.6	61.8	12.4	**2.81**	96.6	59.9	13.6	**2.70**
2	74.4	18.2	20.7	**2.71**	74.4	24.1	20.3	**2.48**
3	67.0	16.2	20.7	**2.45**	67.0	13.6	20.3	**2.63**
Ave.				**2.66±0.19**				**2.60±0.11**

	3-Ni			
Entry	$[MB]_{0,\,aq}$	$[MB]_{1,\,aq}$	[MOSC]	**[MB]/[MOSC]**
1	96.6	67.1	12.6	**2.34**
2	74.4	33.0	22.9	**1.81**
3	67.0	24.2	22.9	**1.87**
Ave.				**2.01±0.29**

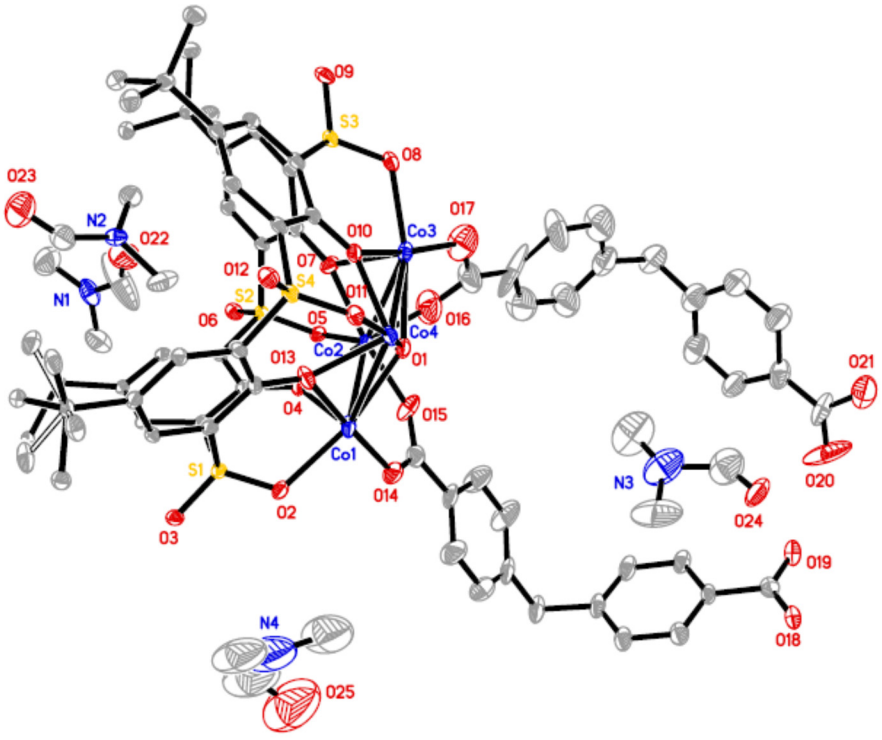

Figure S1. ORTEP drawing of the asymmetric unit of **1-Co** (thermal ellipsoids with 30% probability).

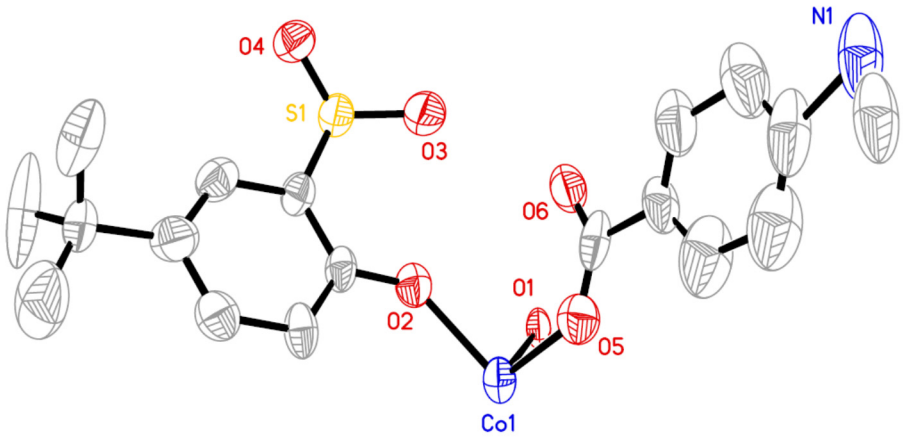

Figure S2. ORTEP drawing of the asymmetric unit of **2-Co** (thermal ellipsoids with 30% probability).

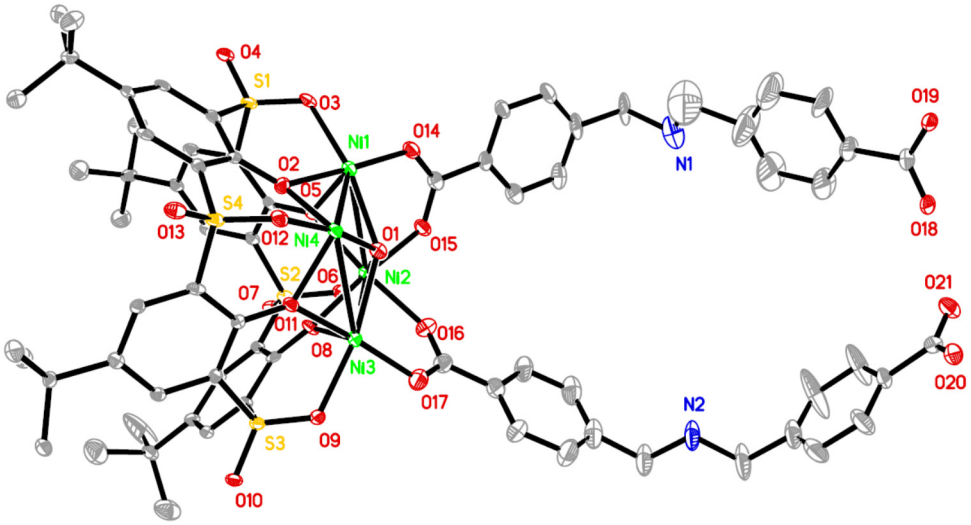

Figure S3. ORTEP drawing of the asymmetric unit of **3-Ni** (thermal ellipsoids with 30% probability).

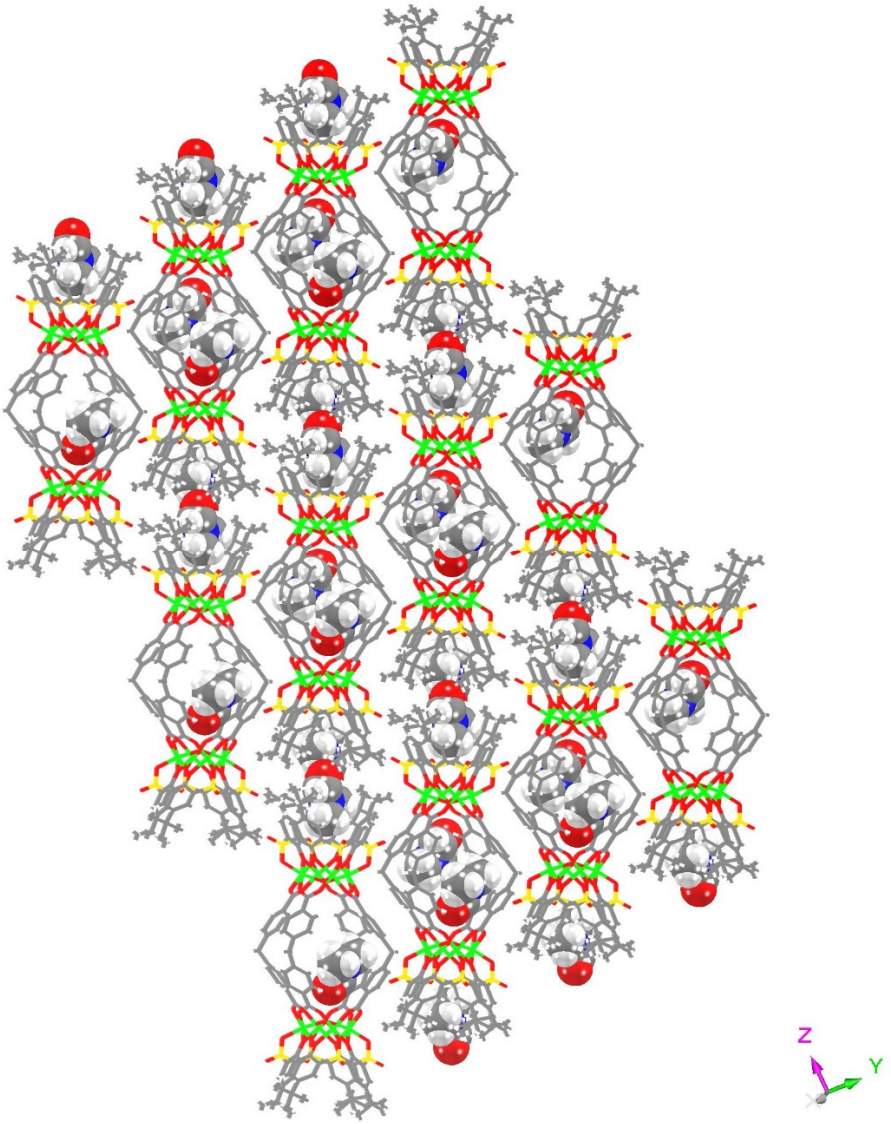

Figure S4. 1D tubular assembly of **1-Co** viewed along the crystallographic *a* axis. The MOSC molecules are shown in wireframe mode and the encapsulated DMF molecules are shown in spacefilling mode. Additional DMF molecules occupying the interstitial space between the 1D tubes are deleted for clarity.

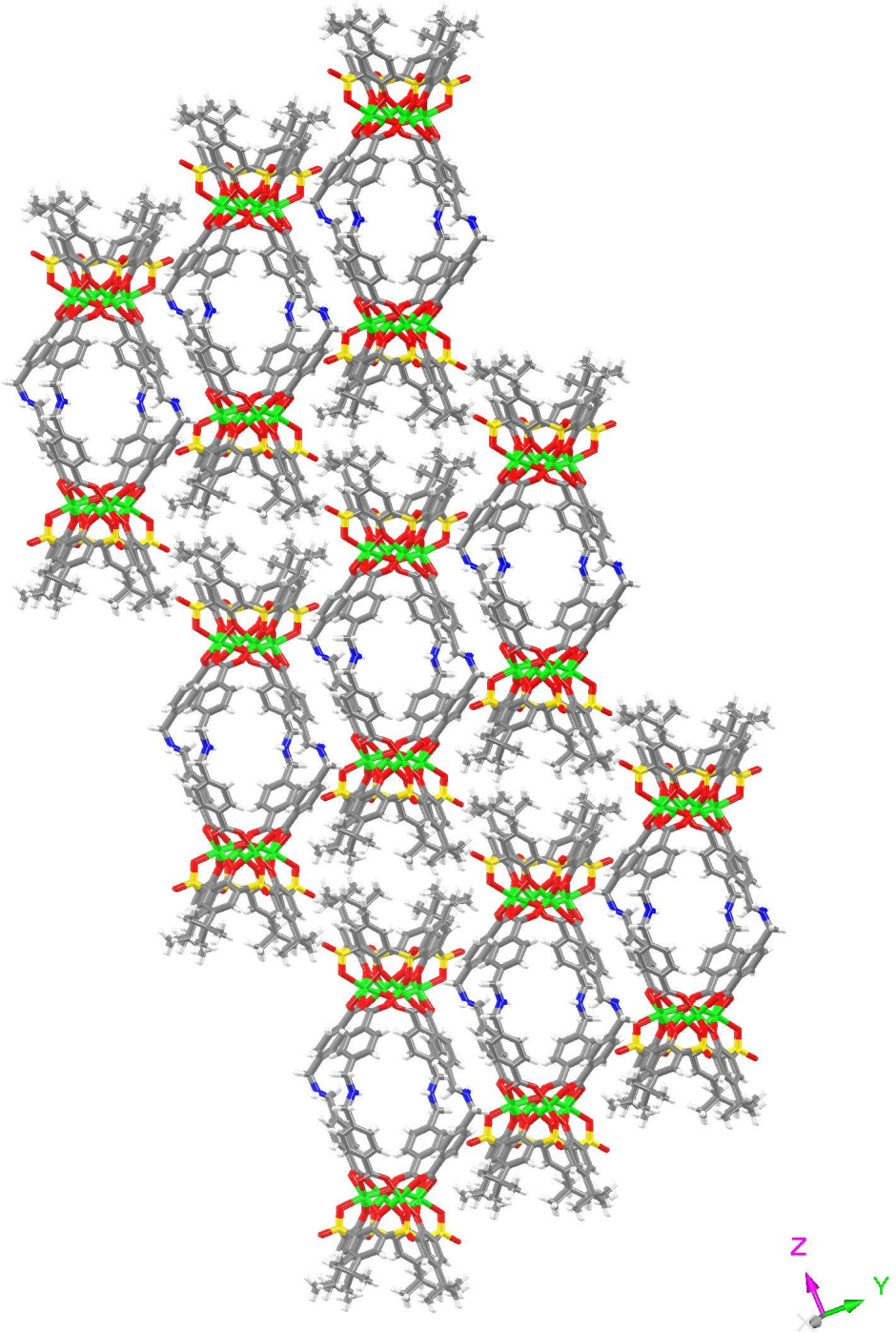

Figure S5. 1D tubular assembly of **3-Ni** viewed along the crystallographic *a* axis. The MOSC molecules are shown in stick mode. The solvent molecules are not included due to the difficulty of precisely locating them by X-ray crystallography as a result of the relatively weak diffraction of the crystals.

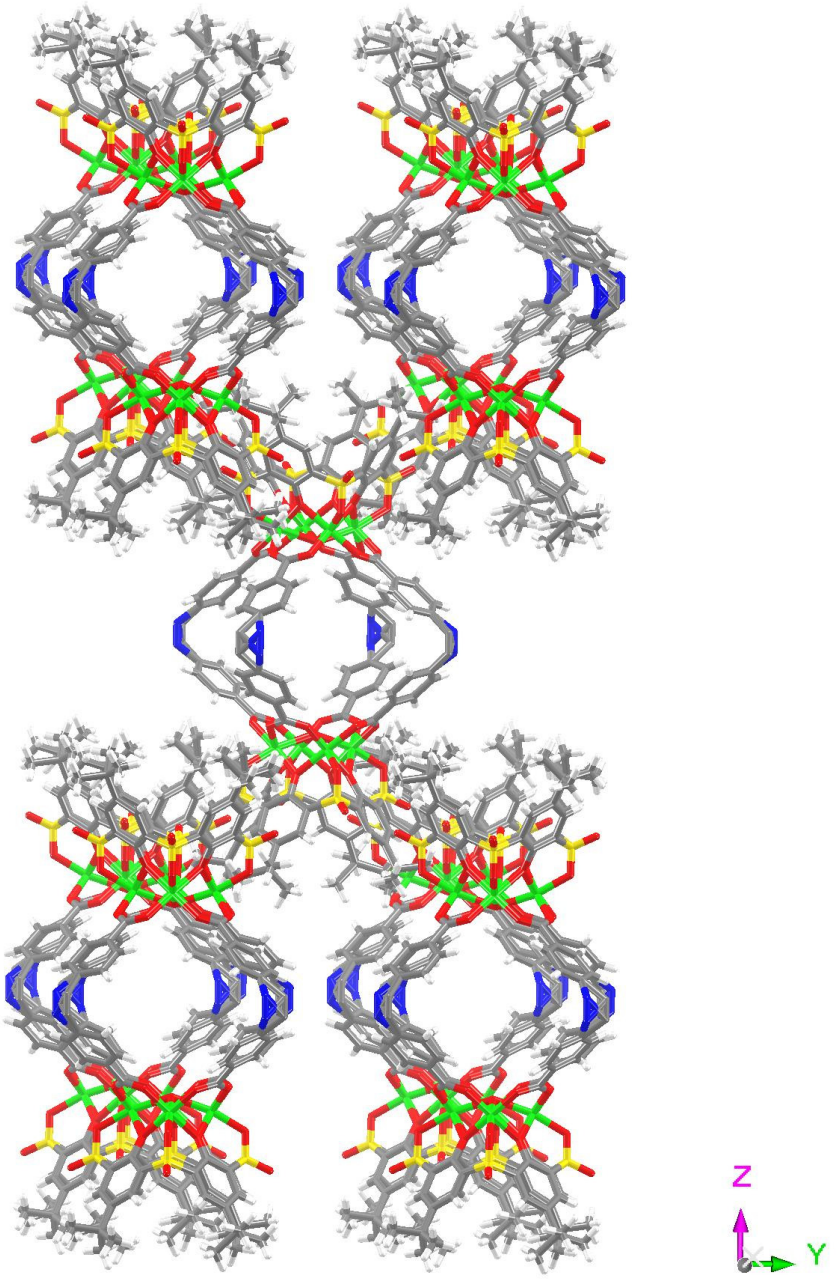

Figure S6. The body-centered cubic (bcc) packing of **2-Co** viewed along the crystallographic *a* axis. The MOSC molecules are shown in stick mode. The solvent molecules are not included due to the difficulty of precisely locating them by X-ray crystallography as a result of the relatively weak diffraction of the crystals.

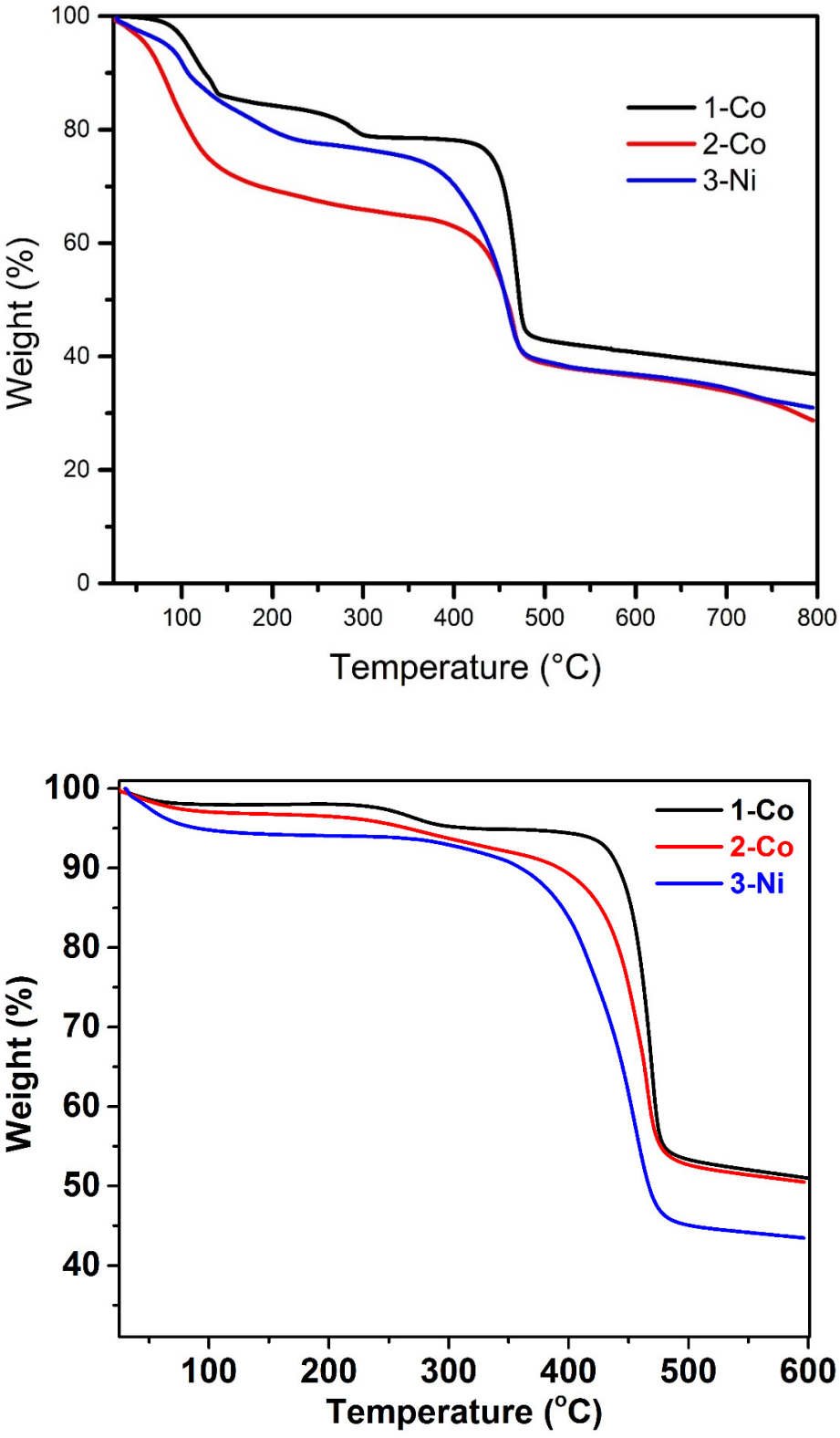

Figure S7. (Top) TGA curves of as-synthesized **1-Co** (black), **2-Co** (red), and **3-Ni** (blue); (bottom) TGA curves of evacuated **1-Co** (black), **2-Co** (red), and **3-Ni** (blue).

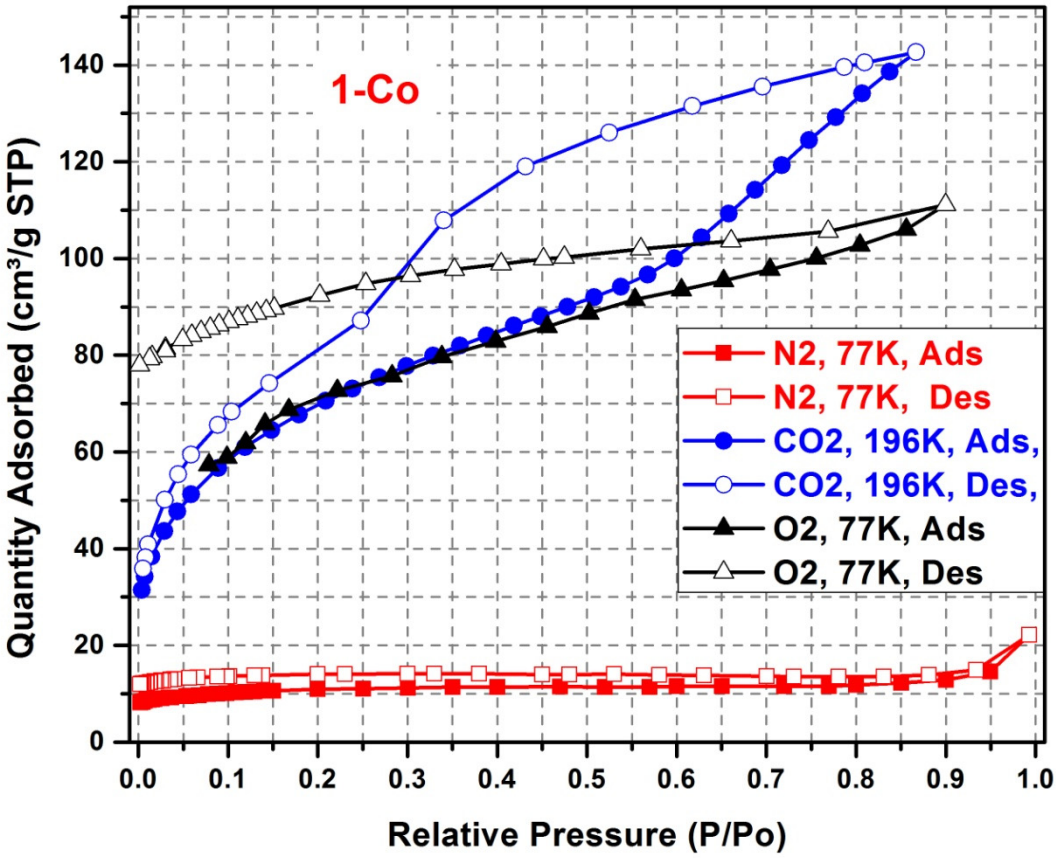

Figure S8. N_2 (77 K), O_2 (77 K), and CO_2 (196 K) sorption isotherms of **1-Co**.

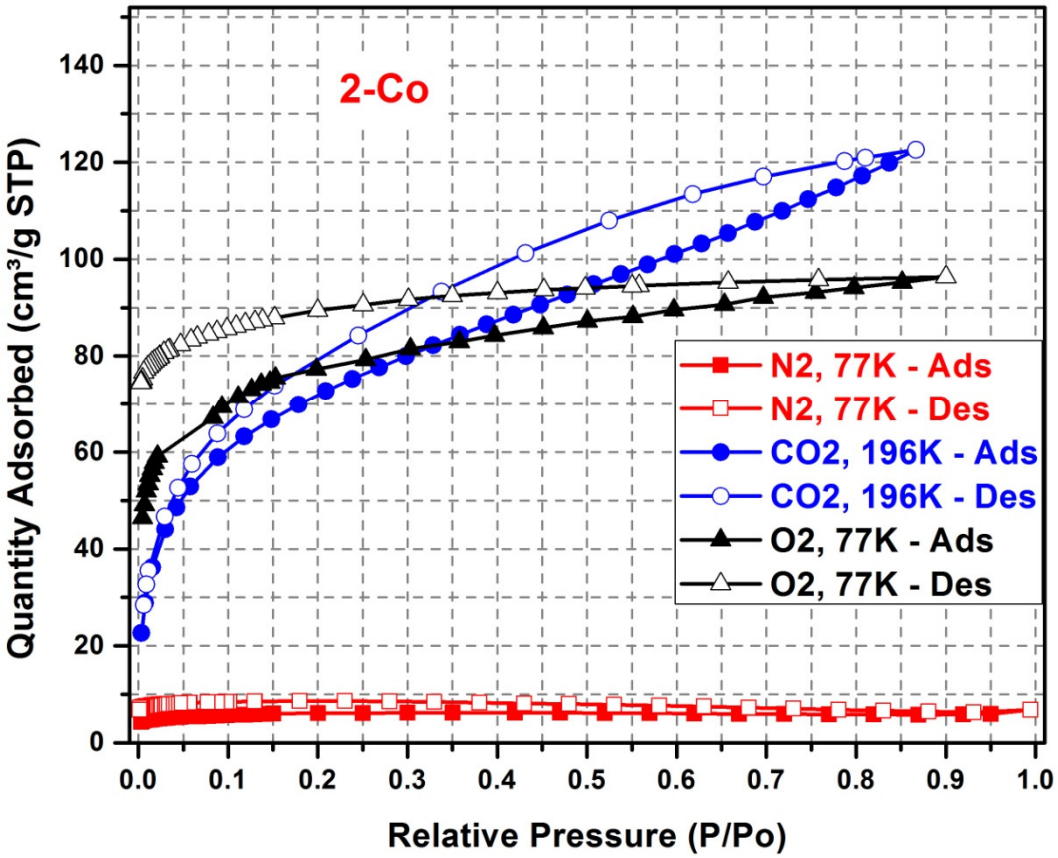

Figure S9. N_2 (77 K), O_2 (77 K), and CO_2 (196 K) sorption isotherms of **2-Co**.

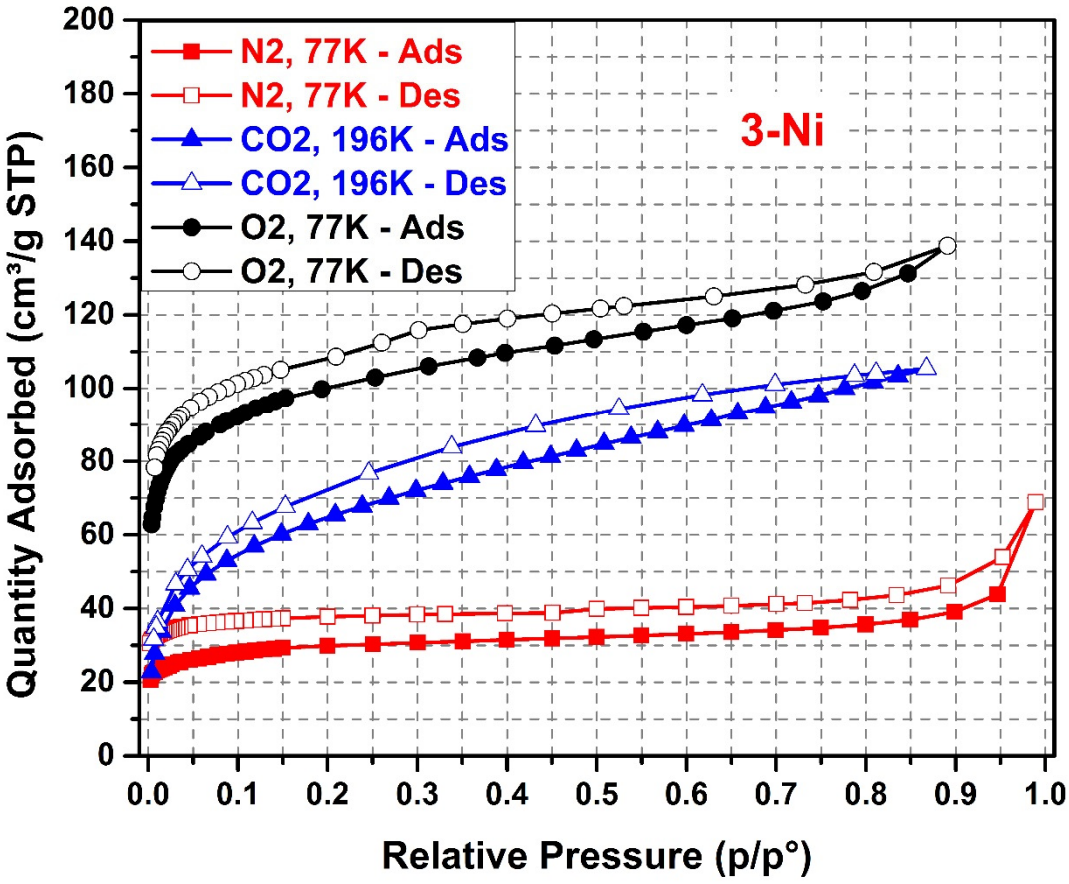

Figure S10. N_2 (77 K), O_2 (77 K), and CO_2 (196 K) sorption isotherms of **3-Ni**.

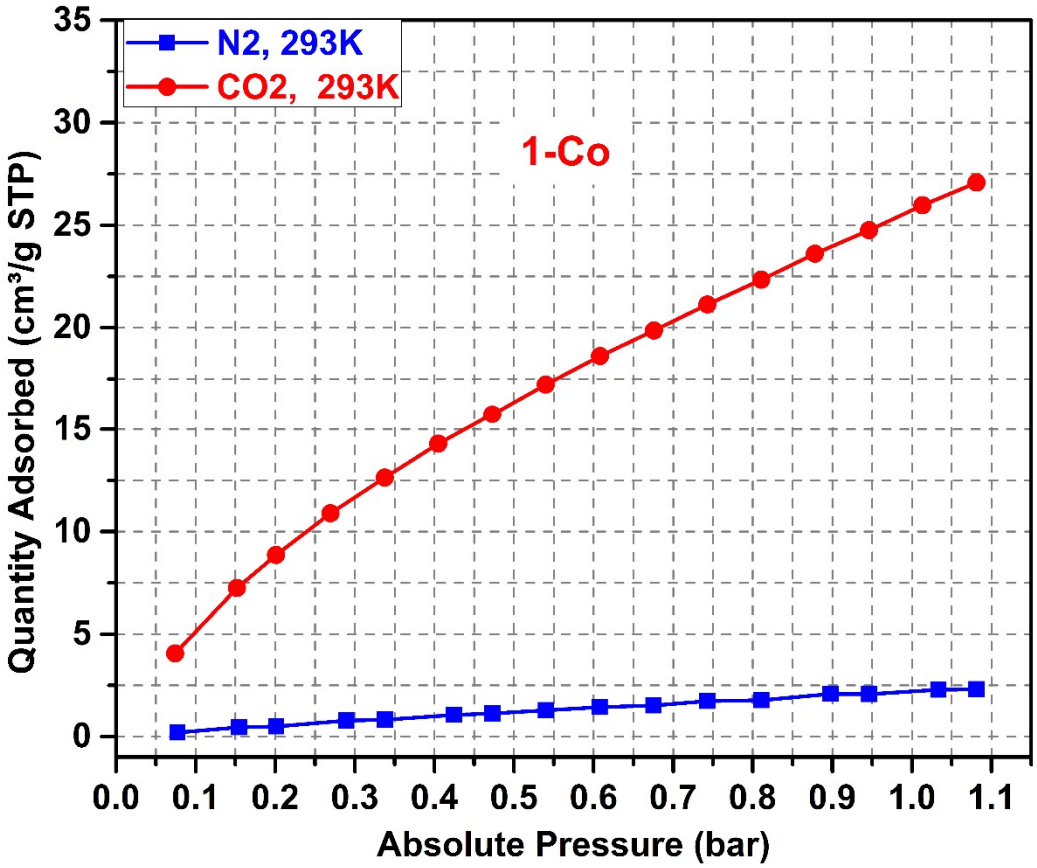

Figure S11. CO_2 and N_2 adsorption isotherms of **1-Co** at ambient conditions.

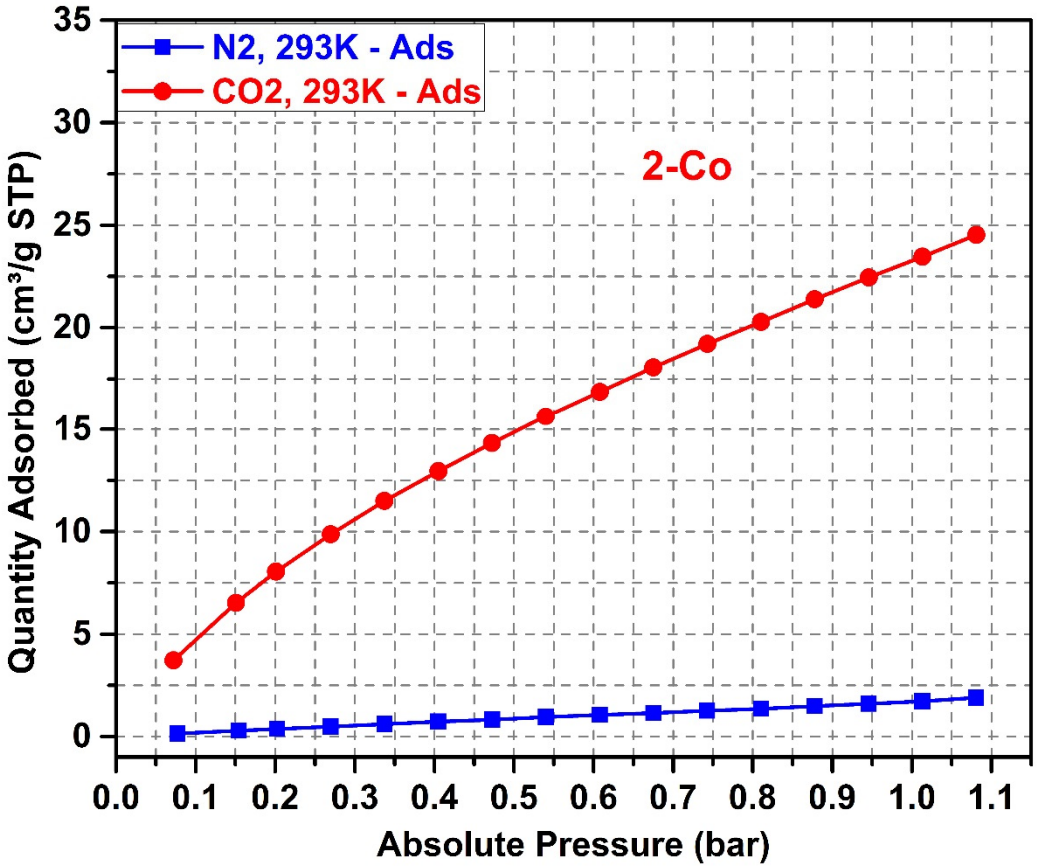

Figure S12. CO_2 and N_2 adsorption isotherms of **2-Co** at ambient conditions.

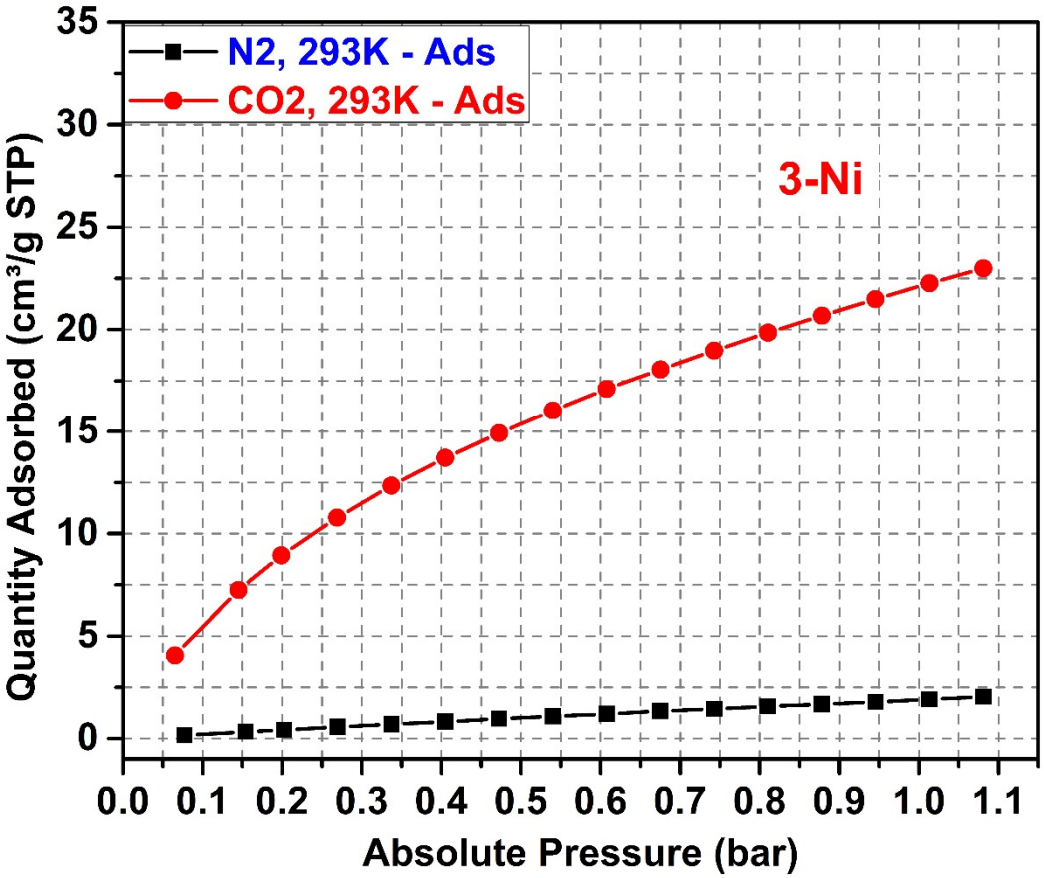

Figure S13. CO_2 and N_2 adsorption isotherms of **3-Ni** at ambient conditions.

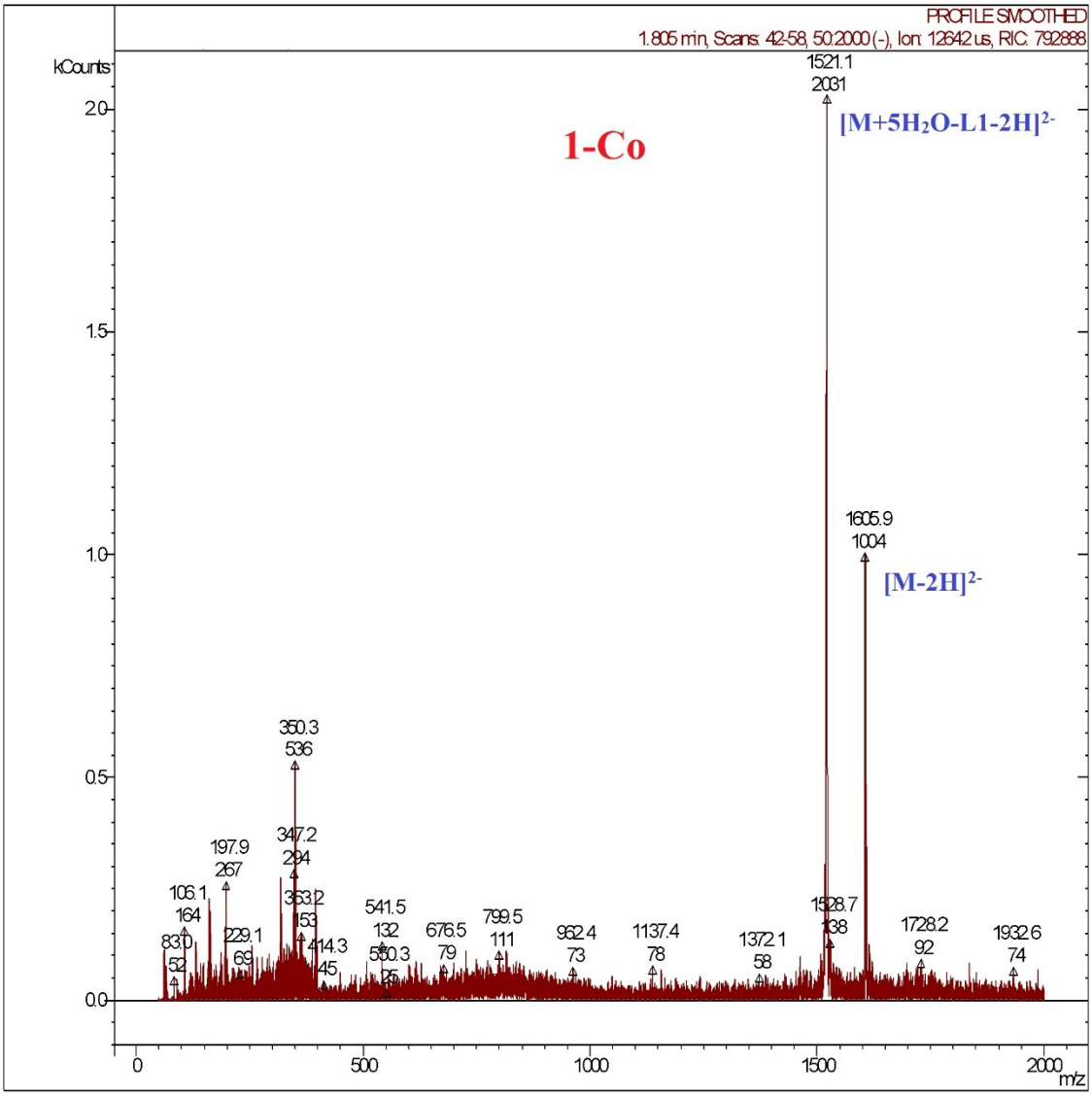

Figure S14. ESI-MS spectrum (negative mode) of **1-Co**, indicating the structural integrity of the compound in solution.

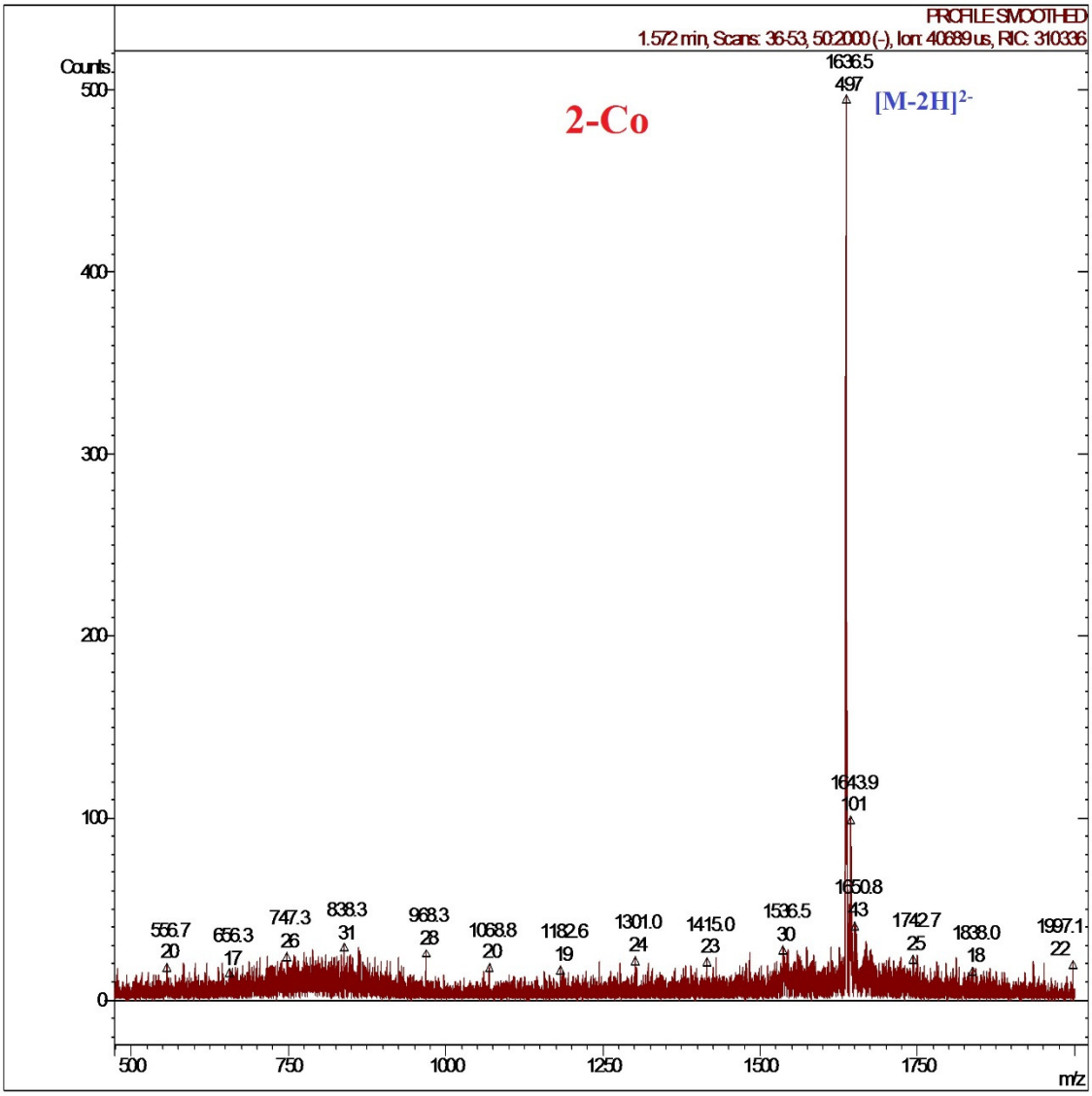

Figure S15. ESI-MS spectrum (negative mode) of **2-Co**, indicating the structural integrity of the compound in solution.

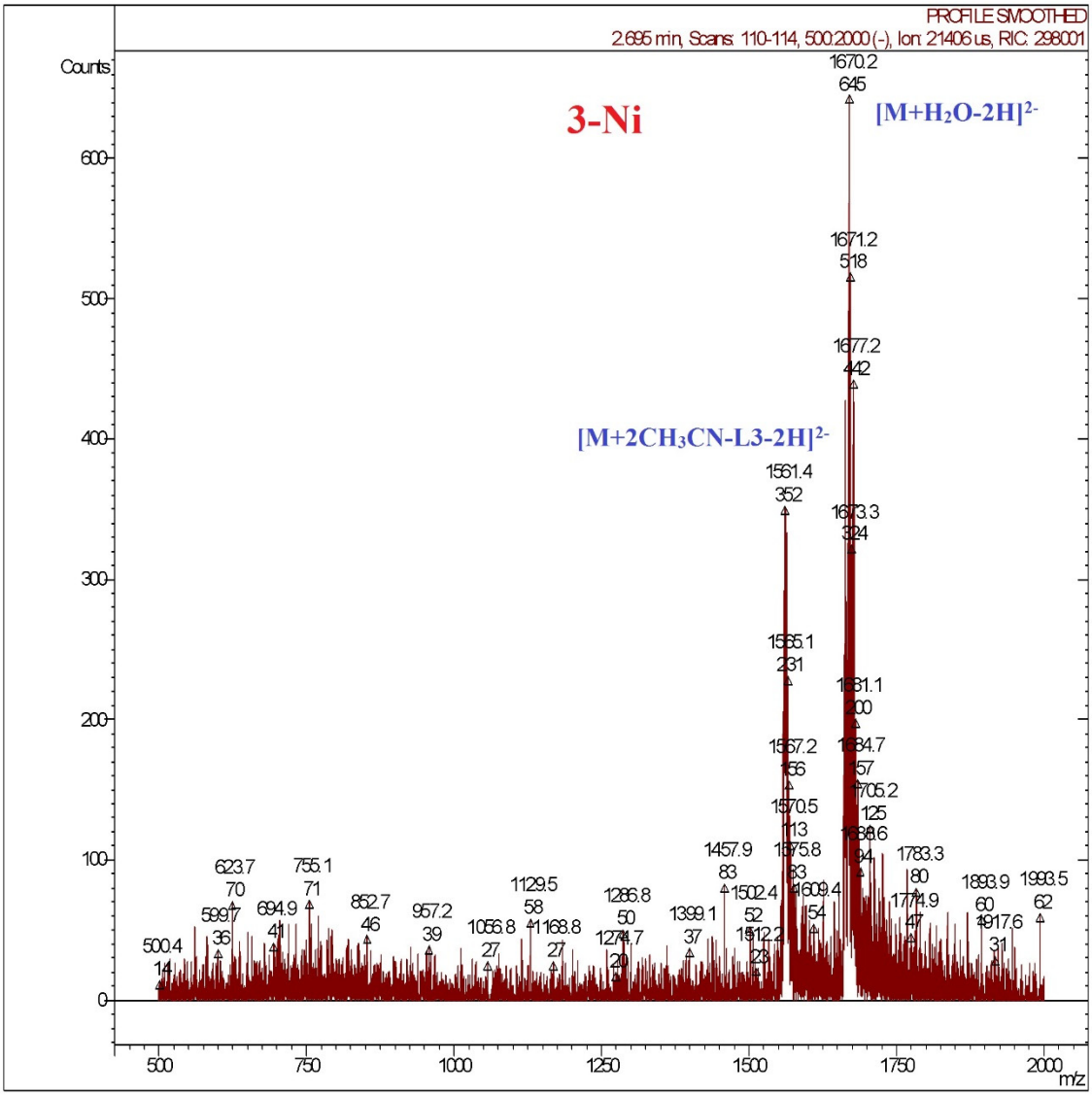

Figure S16. ESI-MS spectrum (negative mode) of **3-Ni**, indicating the structural integrity of the compound in solution.

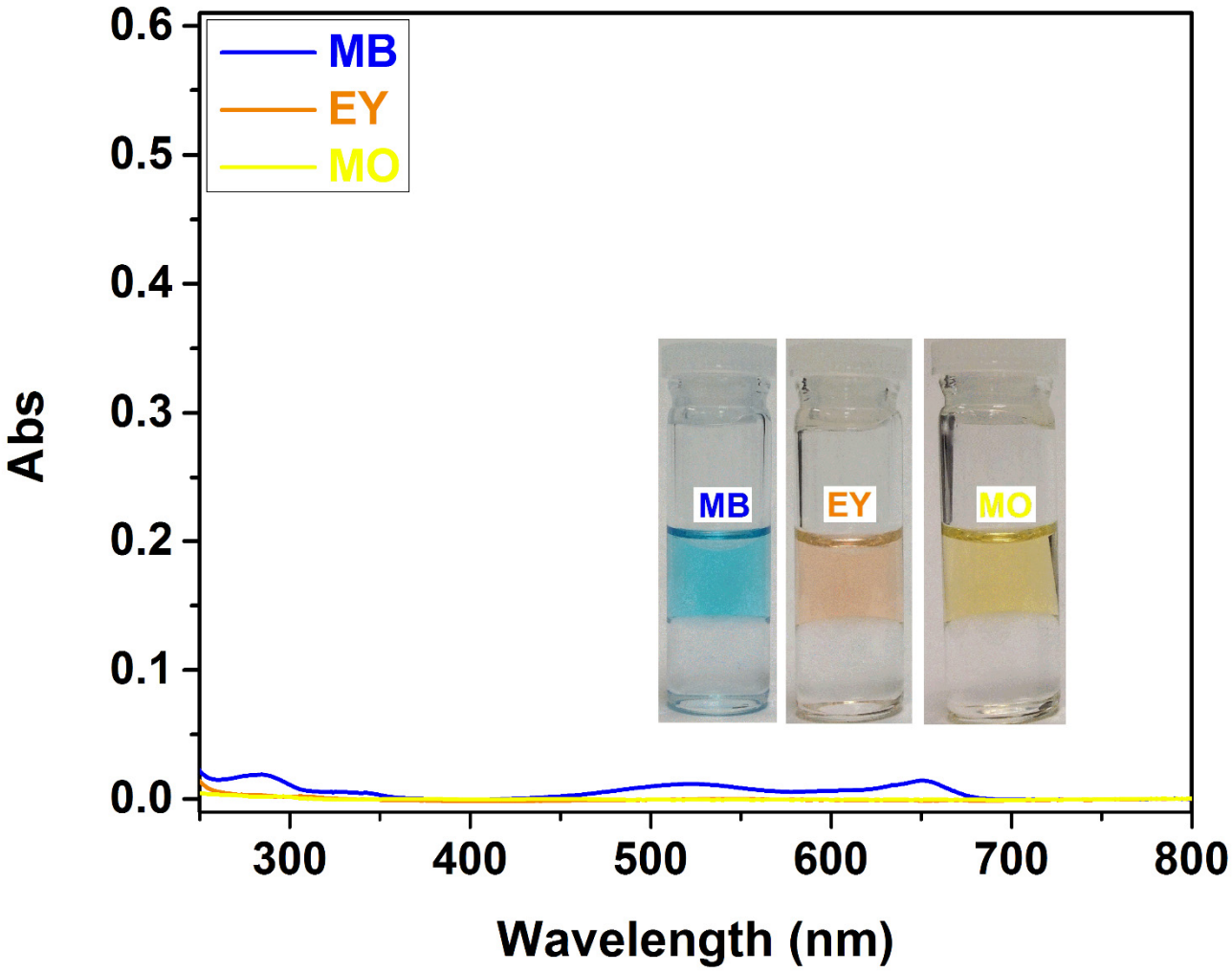

Figure S17. UV-vis spectra of the chloroform solutions (bottom layer) after liquid-liquid (H_2O-$CHCl_3$) extraction of organic dye from aqueous solution to chloroform solution in the absence of MOSCs. The dye, i.e., methylene blue (MB), eosin Y (EY), or methyl orange (MO), was initially dissolved in the aqueous phase (top layer). The inserted photograph indicates no significant extraction for these three dyes.

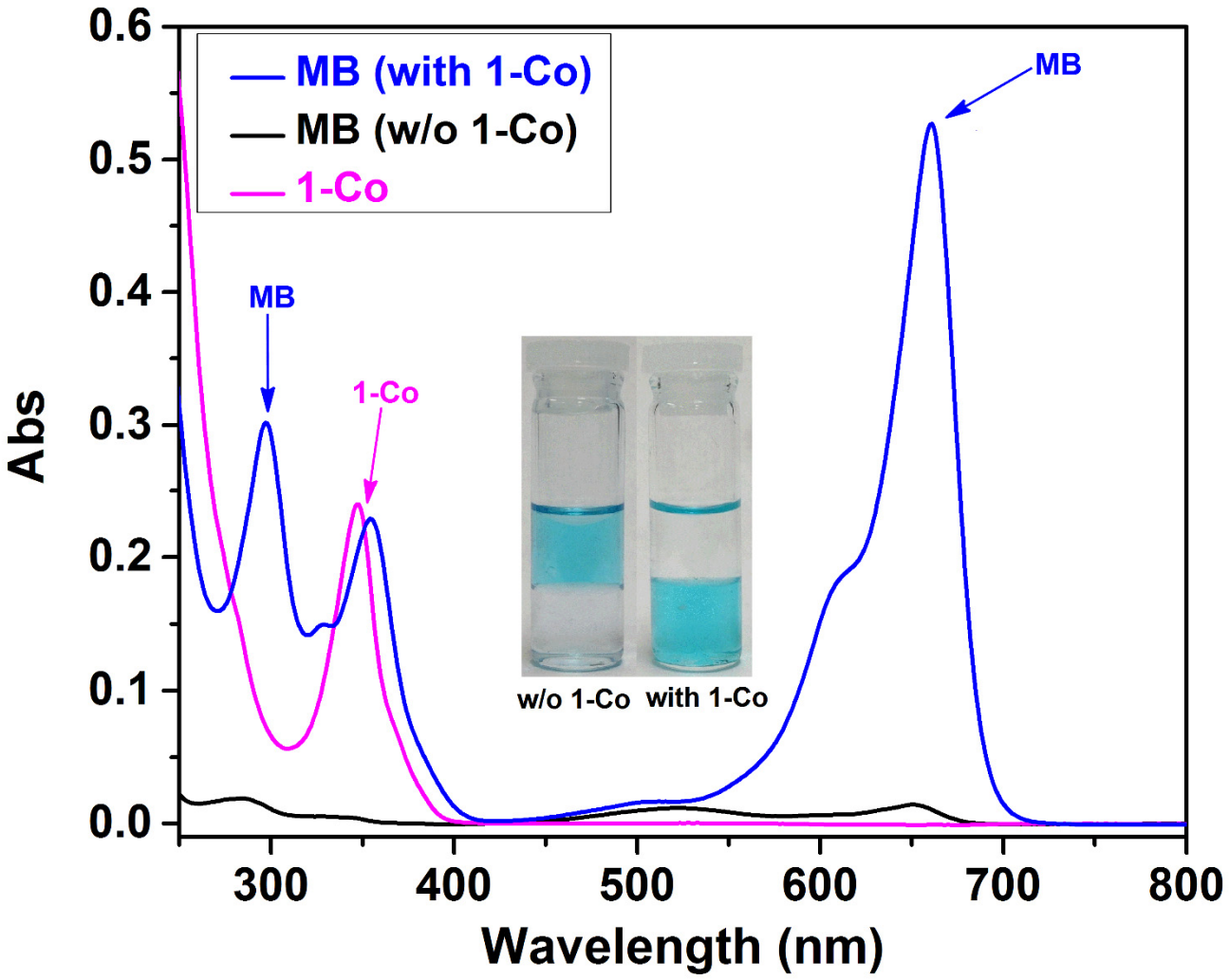

Figure S18. UV-vis spectra of the chloroform solutions after liquid-liquid (H_2O-$CHCl_3$) extraction of MB from aqueous solution to chloroform solution in the presence (blue curve) and absence (black curve) of **1-Co**. The magenta curve represents the UV-vis spectrum of **1-Co** in chloroform before the extraction. The inserted photograph illustrates the liquid-liquid extraction in the absence (left vial) and presence (right vial) of **1-Co**.

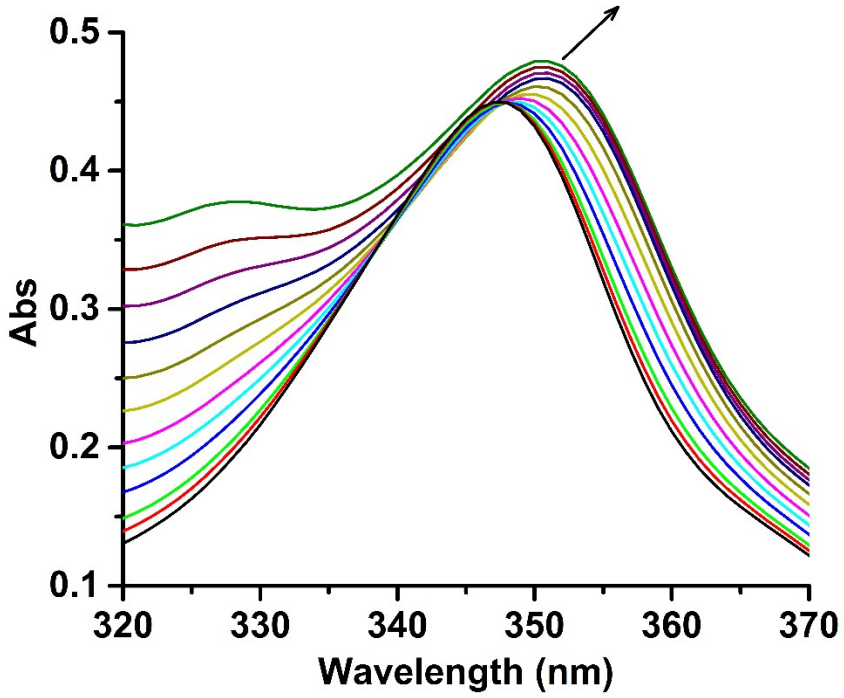

Figure S19. UV-vis spectra of **1-Co** in chloroform upon titration of MB.

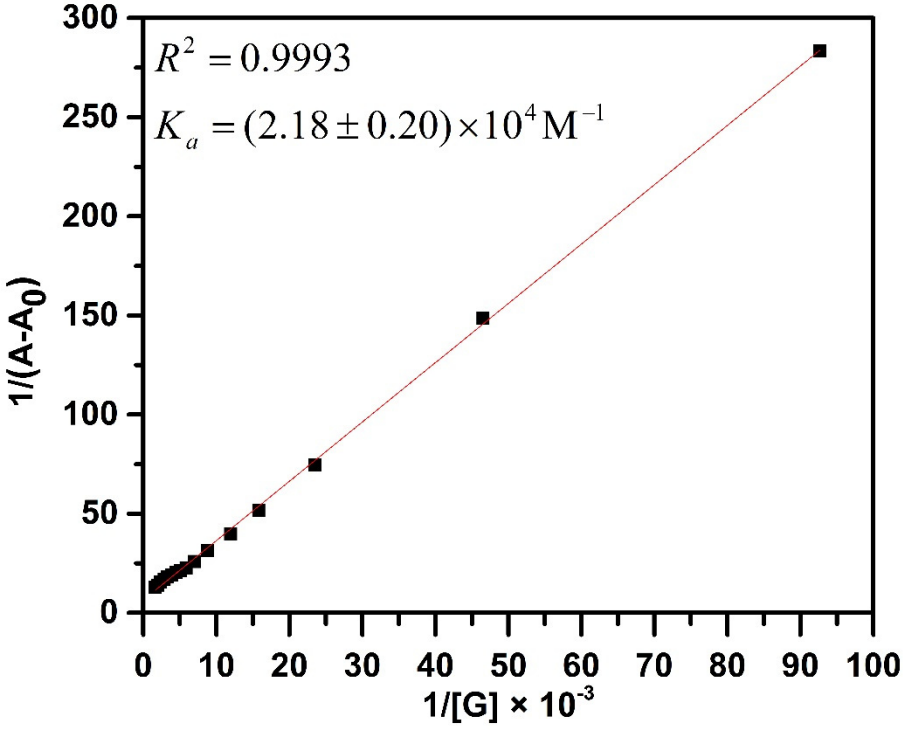

Figure S20. Linear fit of MB/**1-Co** titration data to the Benesi-Hildebrand (B-H) equation.

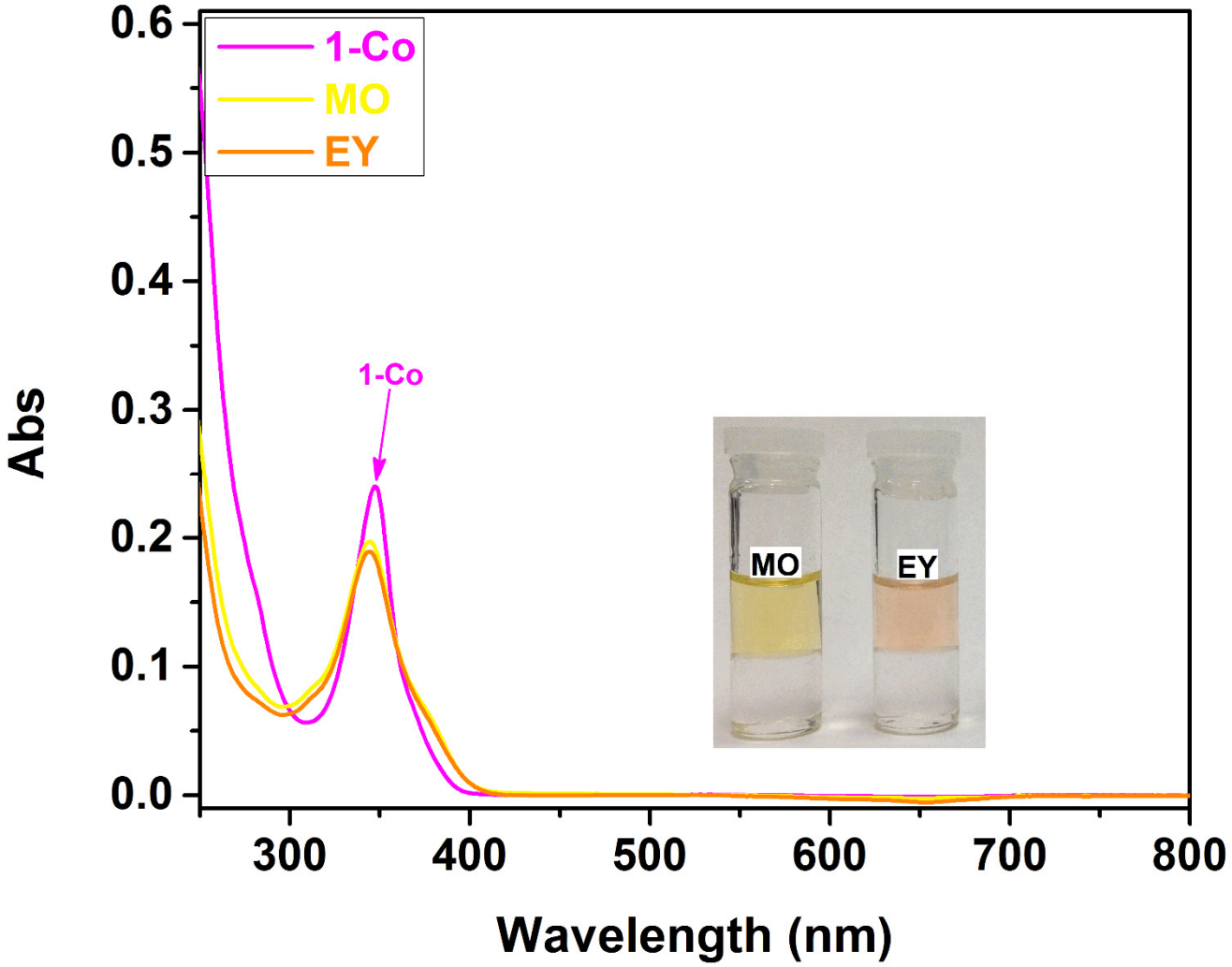

Figure S21. UV-vis spectra of the chloroform solutions after liquid-liquid (H_2O-$CHCl_3$) extraction of eosin Y (EY) and methyl orange (MO) in the presence of **1-Co**. The magenta curve represents the UV-vis spectrum of **1-Co** in chloroform before the extraction. EY and MO were initially dissolved in the aqueous phase (top layer) and **1-Co** was dissolved in the chloroform phase (bottom layer). The spectra and inserted photograph indicate that there is negligible extraction for either dye by **1-Co**.

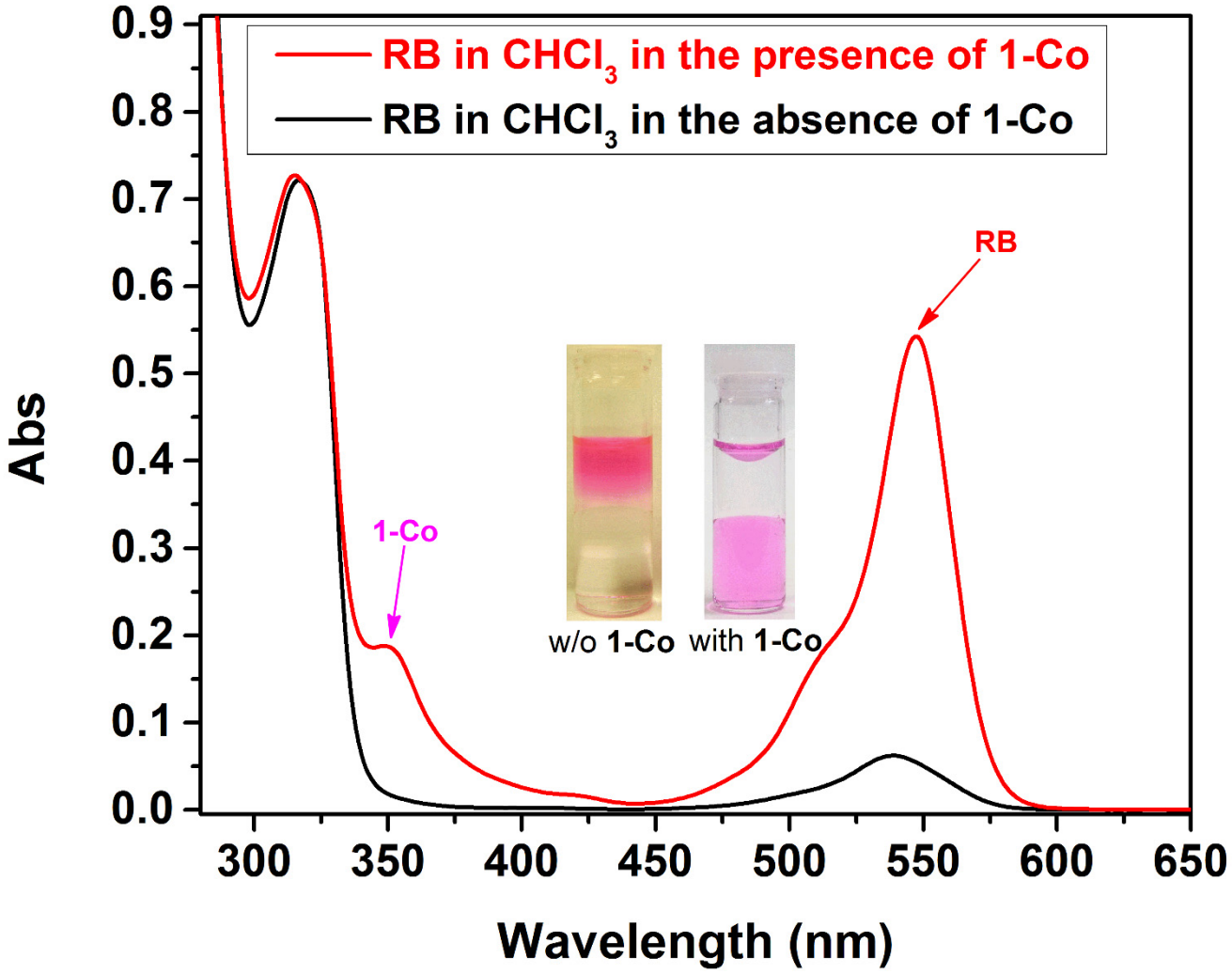

Figure S22. UV-vis spectra of the chloroform solutions after liquid-liquid (H_2O-$CHCl_3$) extraction in the absence (black curve) and presence (red curve) of **1-Co**. The inserted photograph illustrates the extraction experiments (which did not lead to any significant extent of Rhodamine B isomerization; *vide infra*).

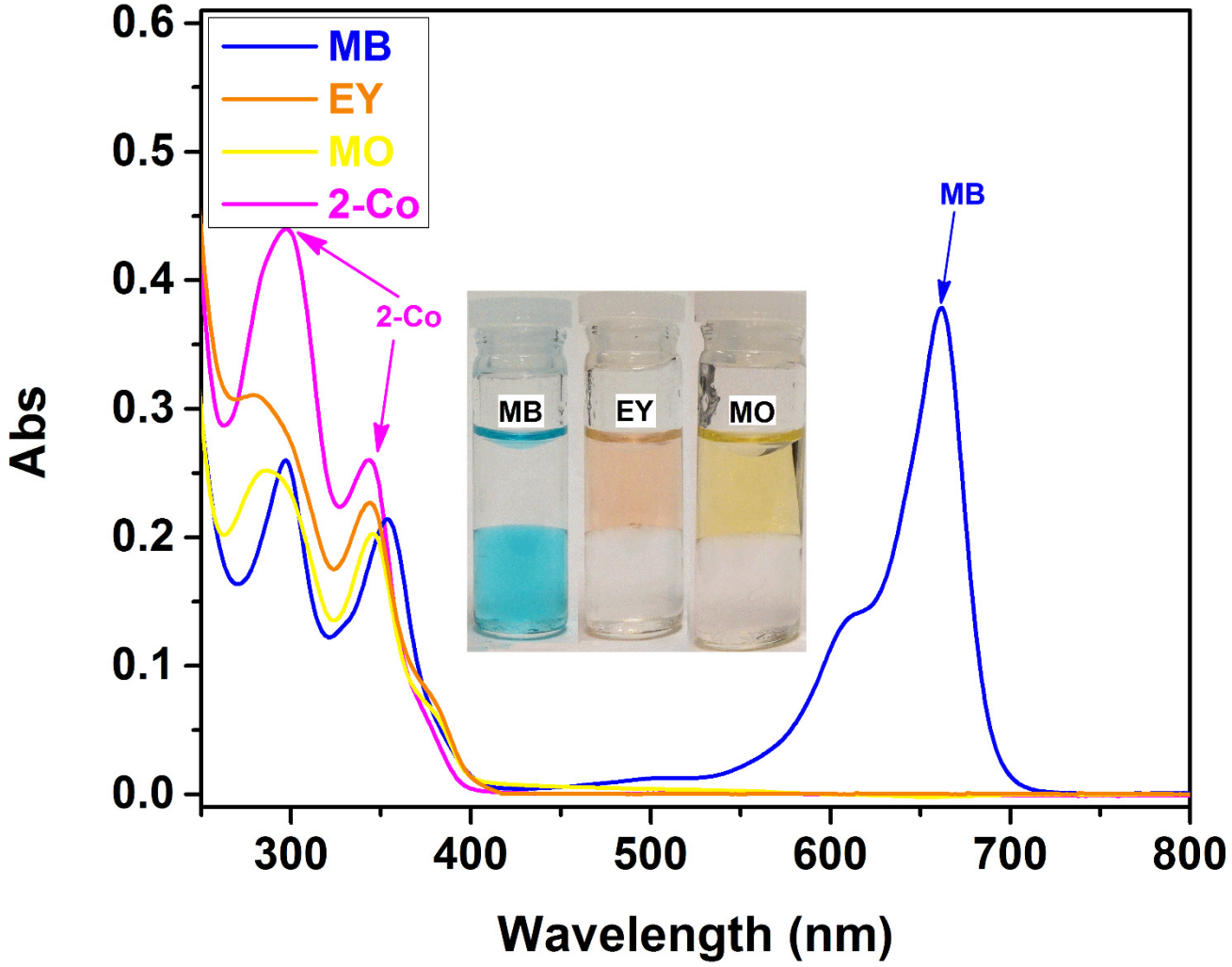

Figure S23. UV-vis spectra of the chloroform solutions after liquid-liquid (H_2O-$CHCl_3$) extraction of MB (blue curve), EY (orange curve), and MO (yellow curve) in the presence of **2-Co**. The magenta curve represents the UV-vis spectrum of **2-Co** in chloroform before the extraction. MB, EY and MO were initially dissolved in the aqueous phase (top layer) and **2-Co** was dissolved in the chloroform phase (bottom layer). The spectra and inserted photograph indicate that there is almost complete extraction for MB but negligible extraction for EY and MO by **2-Co**.

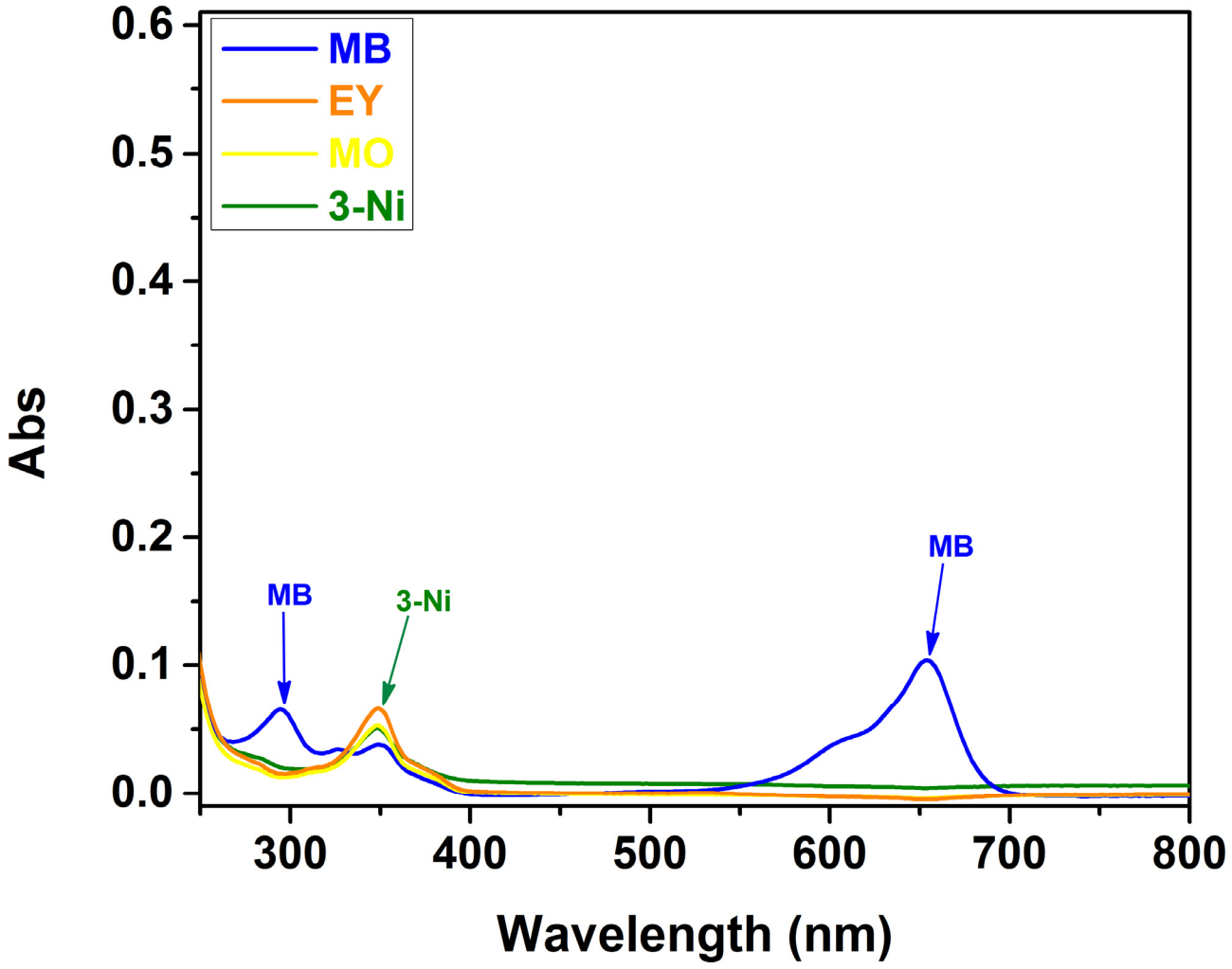

Figure S24. UV-vis spectra of the chloroform solutions after liquid-liquid (H_2O-$CHCl_3$) extraction of MB (blue curve), EY (orange curve), and MO (yellow curve) in the presence of **3-Ni**. The olive curve represents the UV-vis spectrum of **3-Ni** in chloroform before the extraction. MB, EY and MO were initially dissolved in the aqueous phase (top layer) and **3-Ni** was dissolved in the chloroform phase (bottom layer). The spectra indicate that there is substantial (but not complete) extraction for MB but negligible extraction for EY and MO by **3-Ni**.

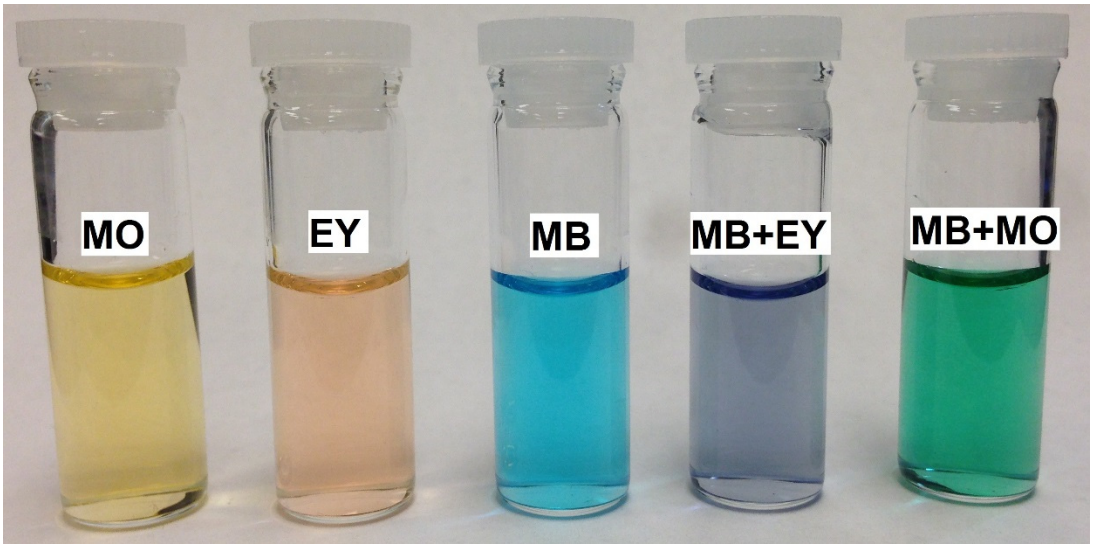

Figure S25. Photographs of aqueous dye solutions. From left to right: MO, EY, MB, MB-EY (1:1), and MB-MO (1:1), respectively.

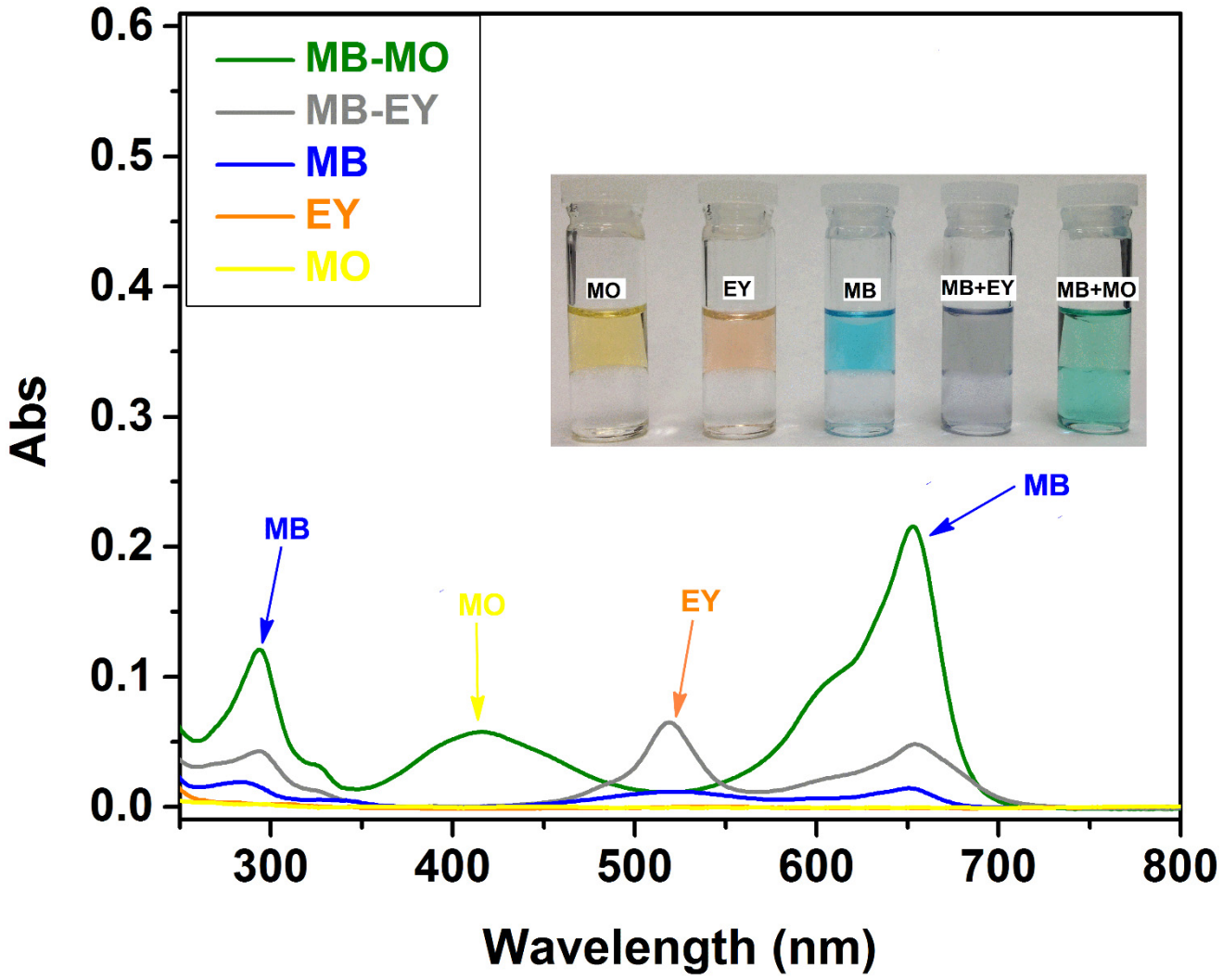

Figure S26. UV-vis spectra of the chloroform solutions after liquid-liquid (H_2O-$CHCl_3$) extraction of MB-MO (olive curve) and MB-EY (gray curve), in the absence of any MOSC, in comparison with those of MB (blue curve), EY (orange curve), and MO (yellow curve). The spectra and inserted photograph illustrate the enhanced solubility of the dye mixtures in chloroform.

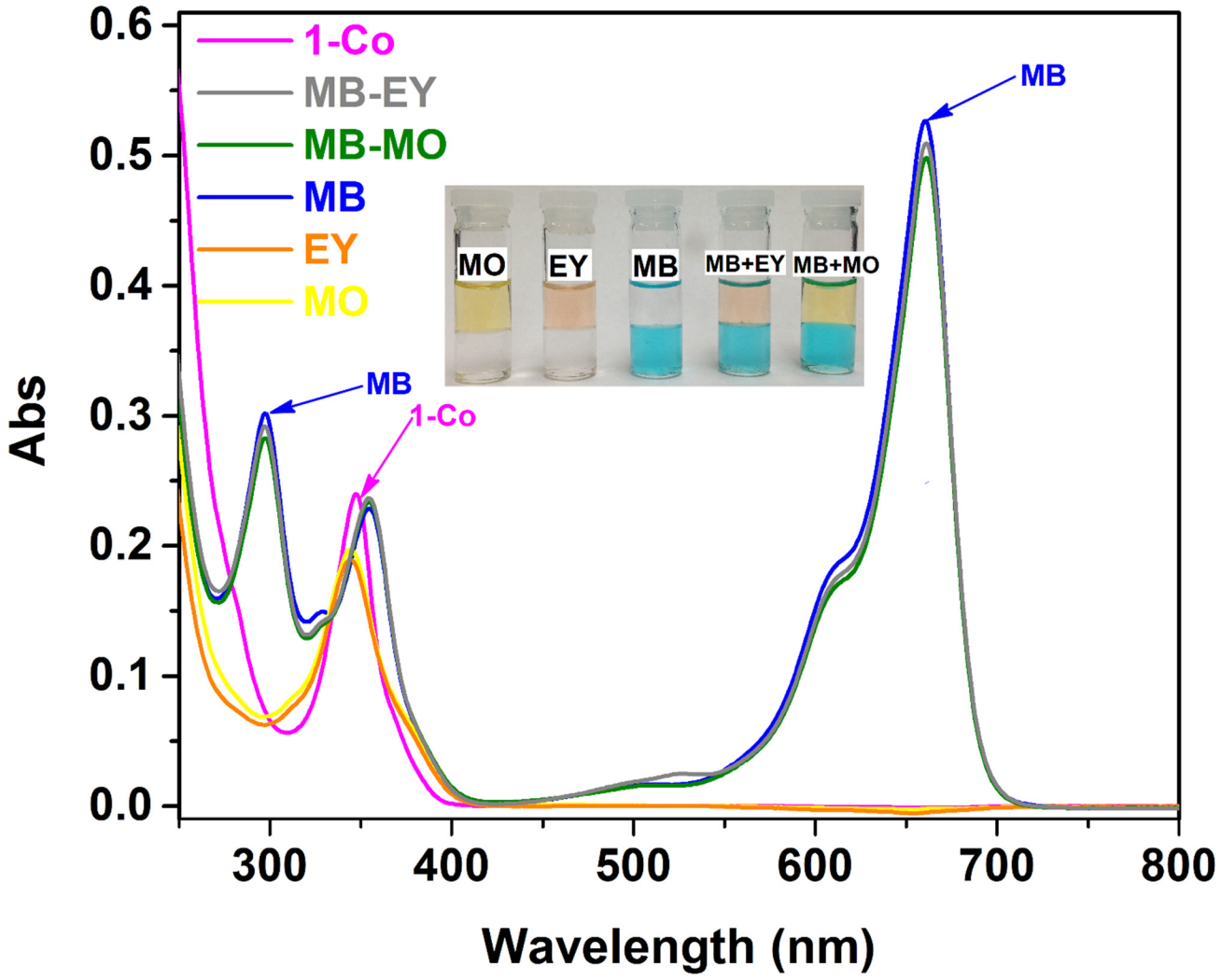

Figure S27. UV-vis spectra of the chloroform solutions after liquid-liquid (H_2O-$CHCl_3$) extraction of MB-EY (gray curve) and MB-MO (olive curve), in the presence of **1-Co**, in comparison with those of MB (blue curve), EY (orange curve), and MO (yellow curve). The magenta curve represents the UV-vis spectrum of **1-Co** in chloroform before the extraction. The inserted photograph illustrates the separation of MB from EY or MO in the binary dye mixtures.

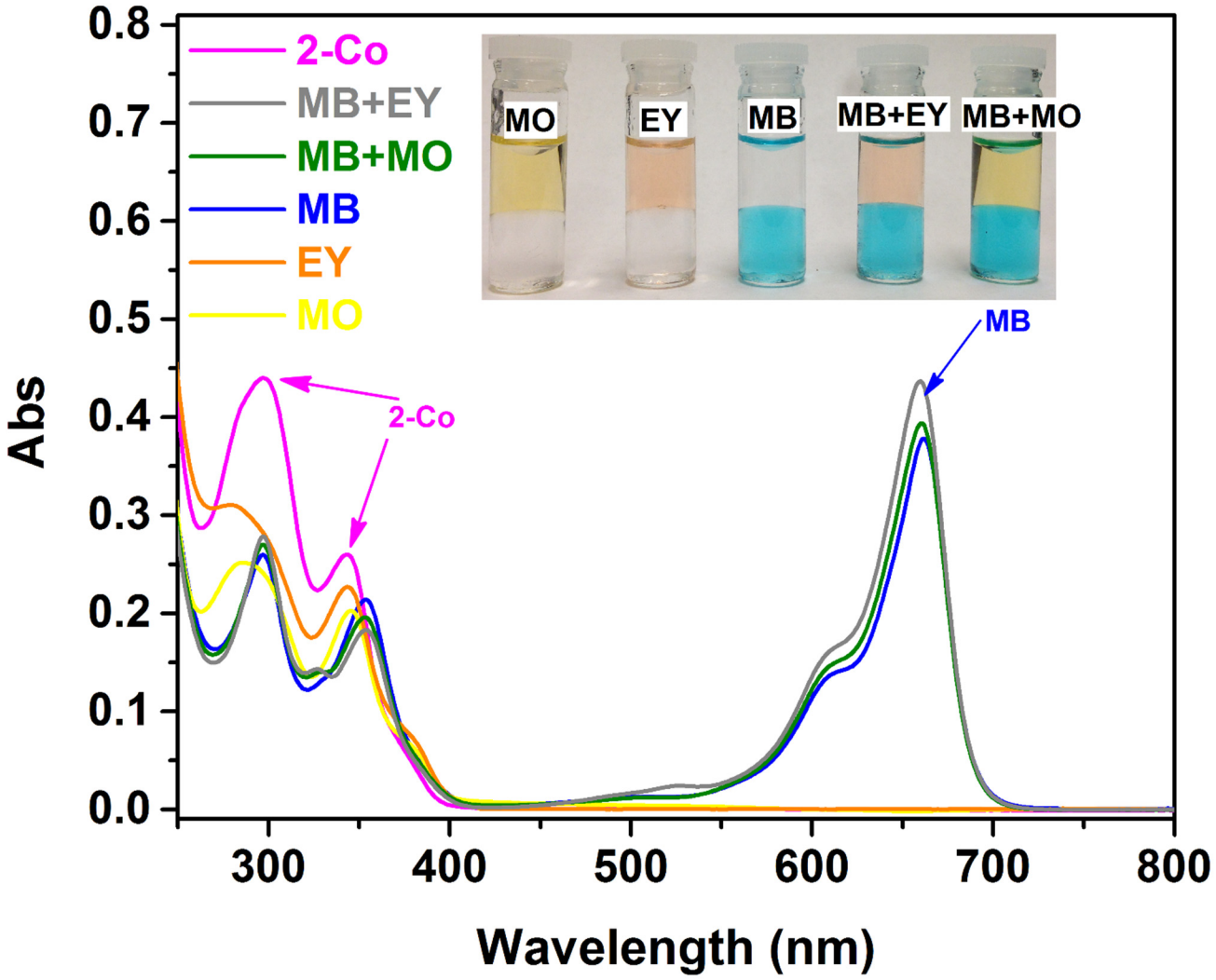

Figure S28. UV-vis spectra of the chloroform solutions after liquid-liquid (H_2O-$CHCl_3$) extraction of MB-EY (gray curve) and MB-MO (olive curve), in the presence of **2-Co**, in comparison with those of MB (blue curve), EY (orange curve), and MO (yellow curve). The magenta curve represents the UV-vis spectrum of **2-Co** in chloroform before the extraction. The inserted photograph illustrates the separation of MB from EY or MO in the binary dye mixtures.

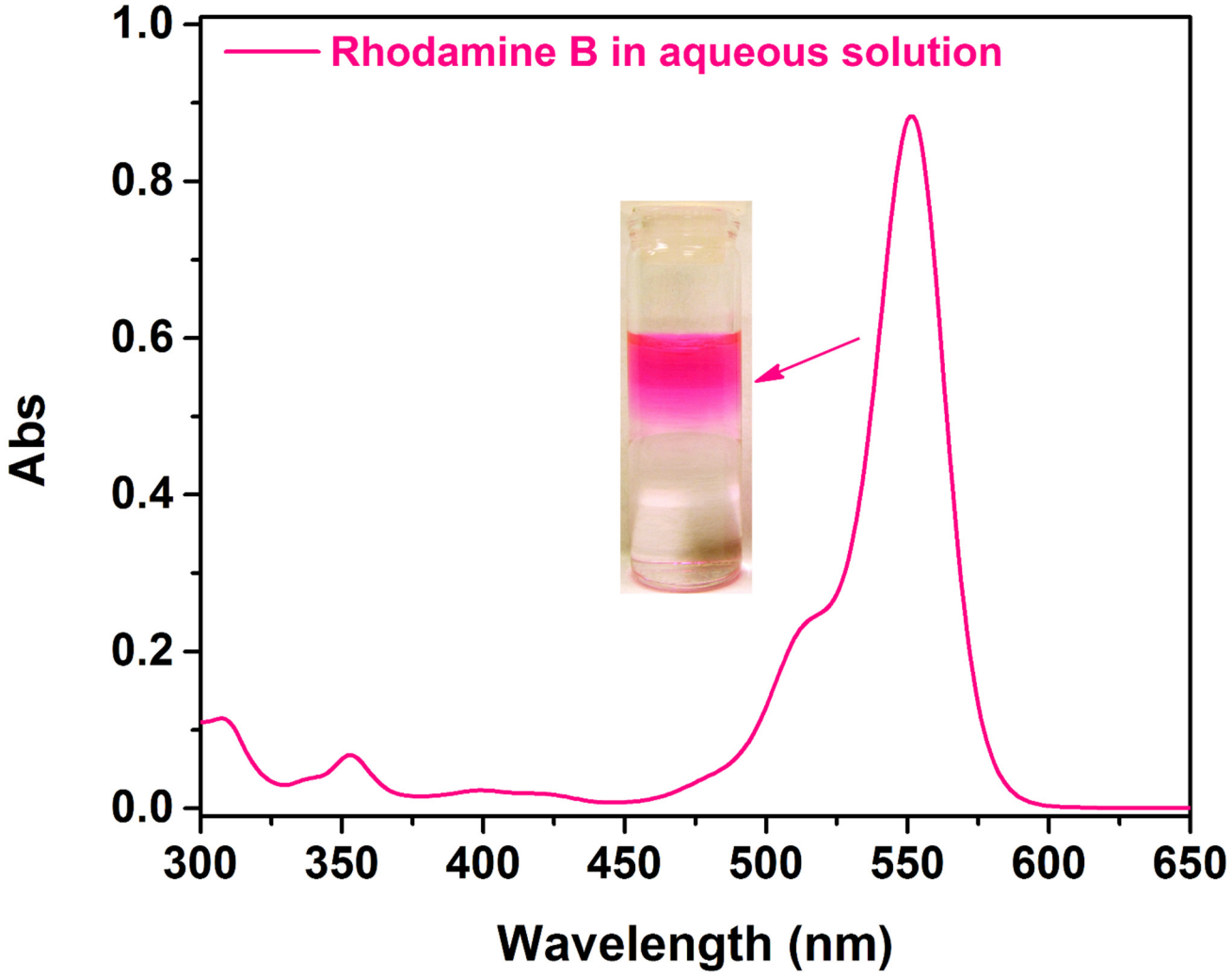

Figure S29. UV-vis spectrum of Rhodamine B in the aqueous solution before liquid-liquid (H_2O-$CHCl_3$) extraction (in the absence of any MOSC).

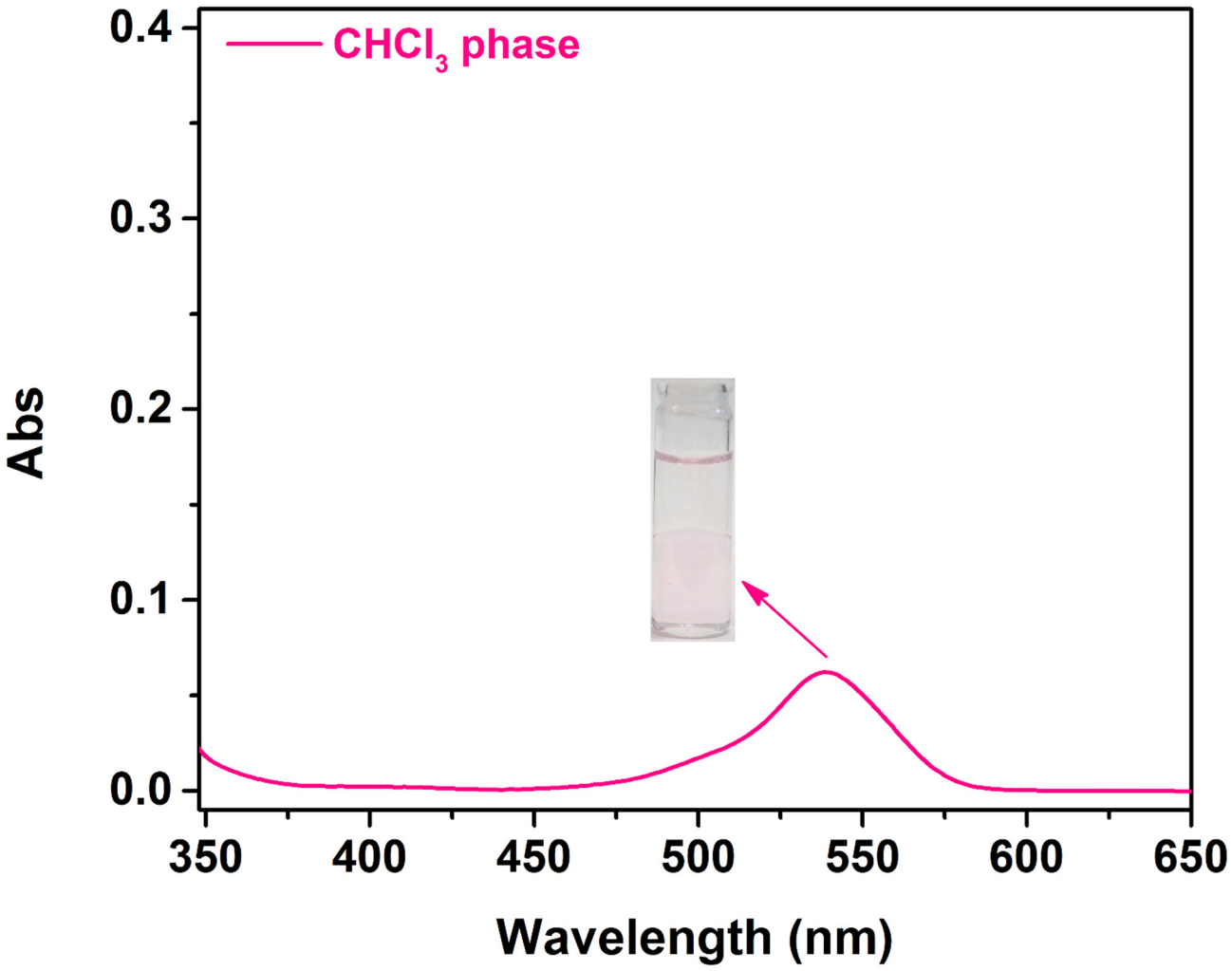

Figure S30. UV-vis spectrum of the chloroform phase (in the absence of any MOSC) after Rhodamine B, initially dissolved in the aqueous phase, was let sit for a long period of time.

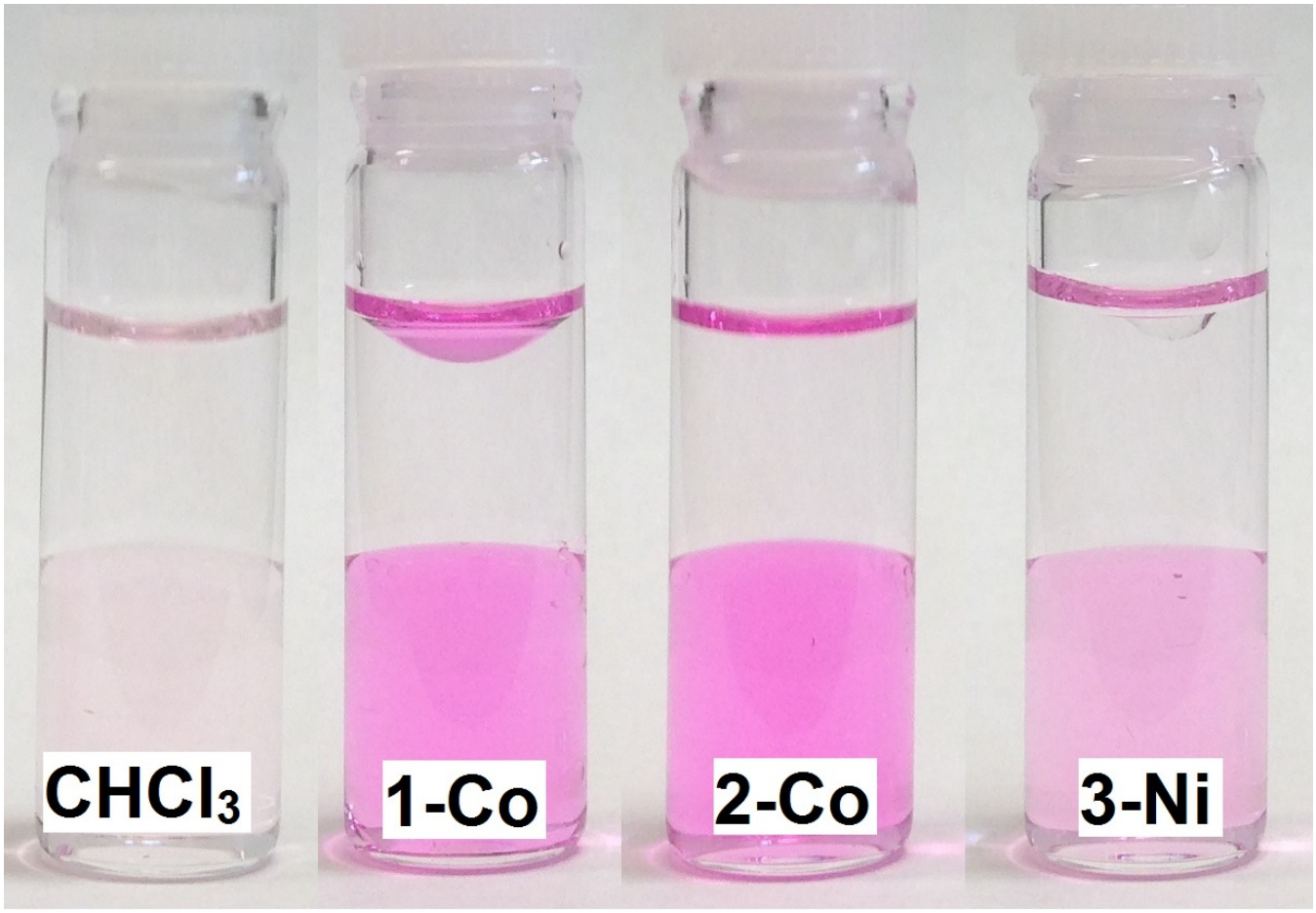

Figure S31. Photographs of liquid-liquid (H_2O-$CHCl_3$) extractions of Rhodamine B dye. From left to right: extraction with straight $CHCl_3$, **1-Co** in $CHCl_3$, **2-Co** in $CHCl_3$, and **3-Ni** in $CHCl_3$, respectively.

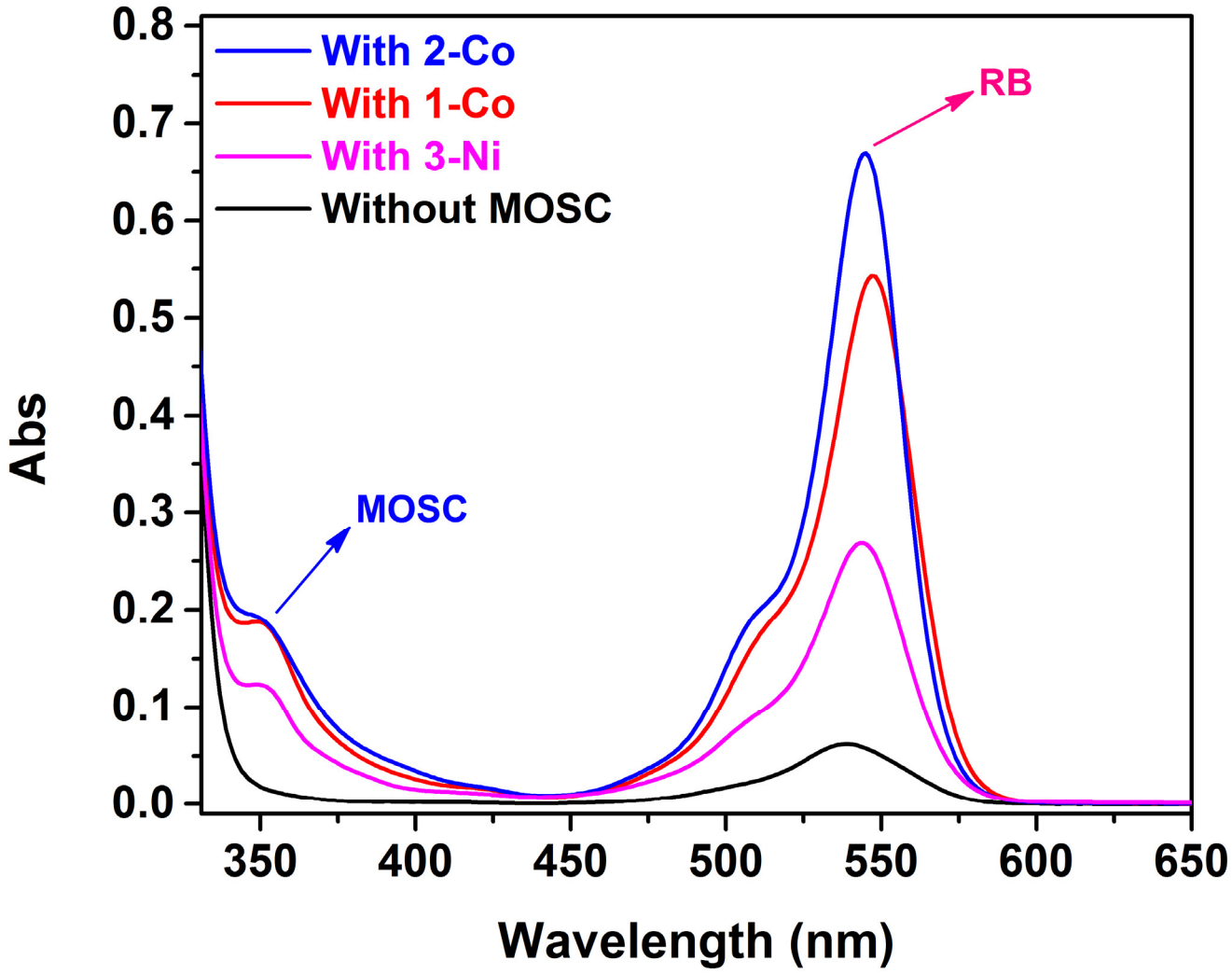

Figure S32. UV-vis spectra of the $CHCl_3$ phase after the extraction of Rhodamine B dye from the aqueous phase to the organic phase by straight $CHCl_3$ (black curve), **1-Co** in $CHCl_3$ (red curve), **2-Co** in $CHCl_3$ (blue curve), and **3-Ni** in $CHCl_3$ (magenta curve), respectively.

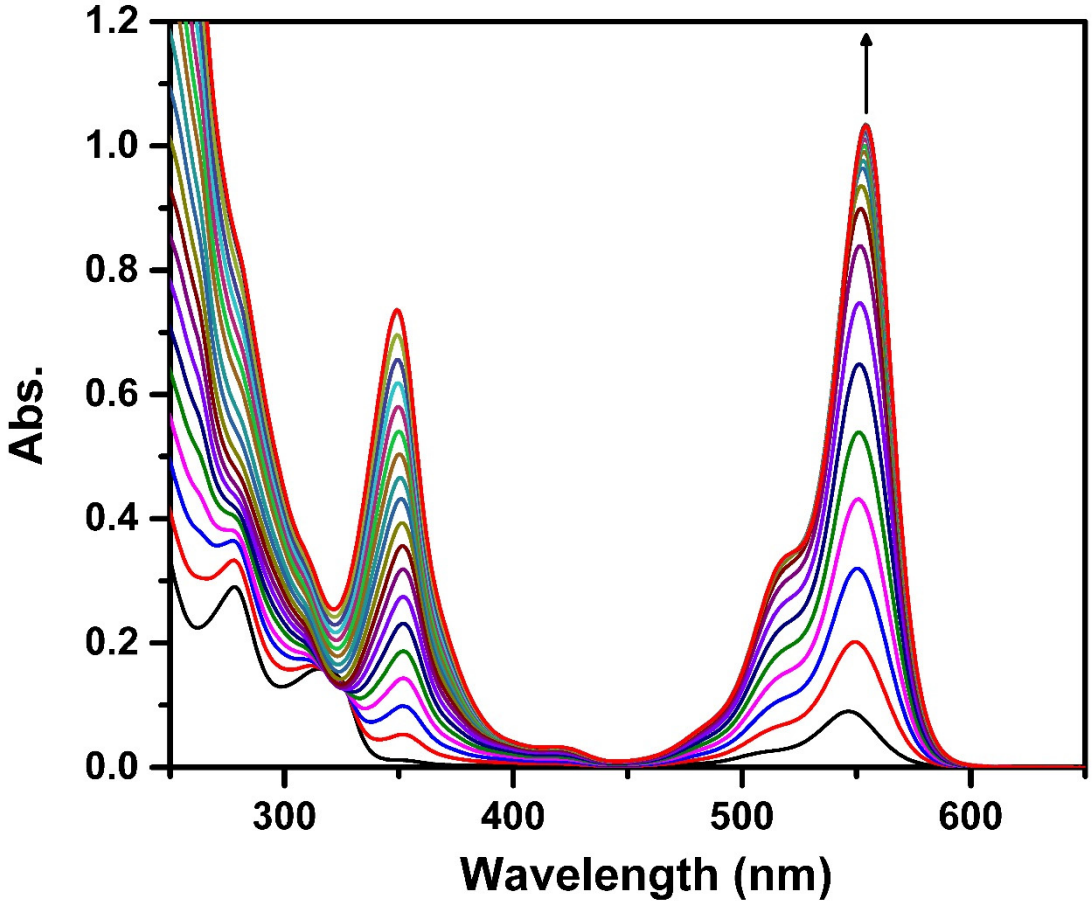

Figure S33. UV-vis absorption curves of Rhodamine B base titrated with **1-Co**. The arrow indicates the gradual increase of **1-Co** equivalents.

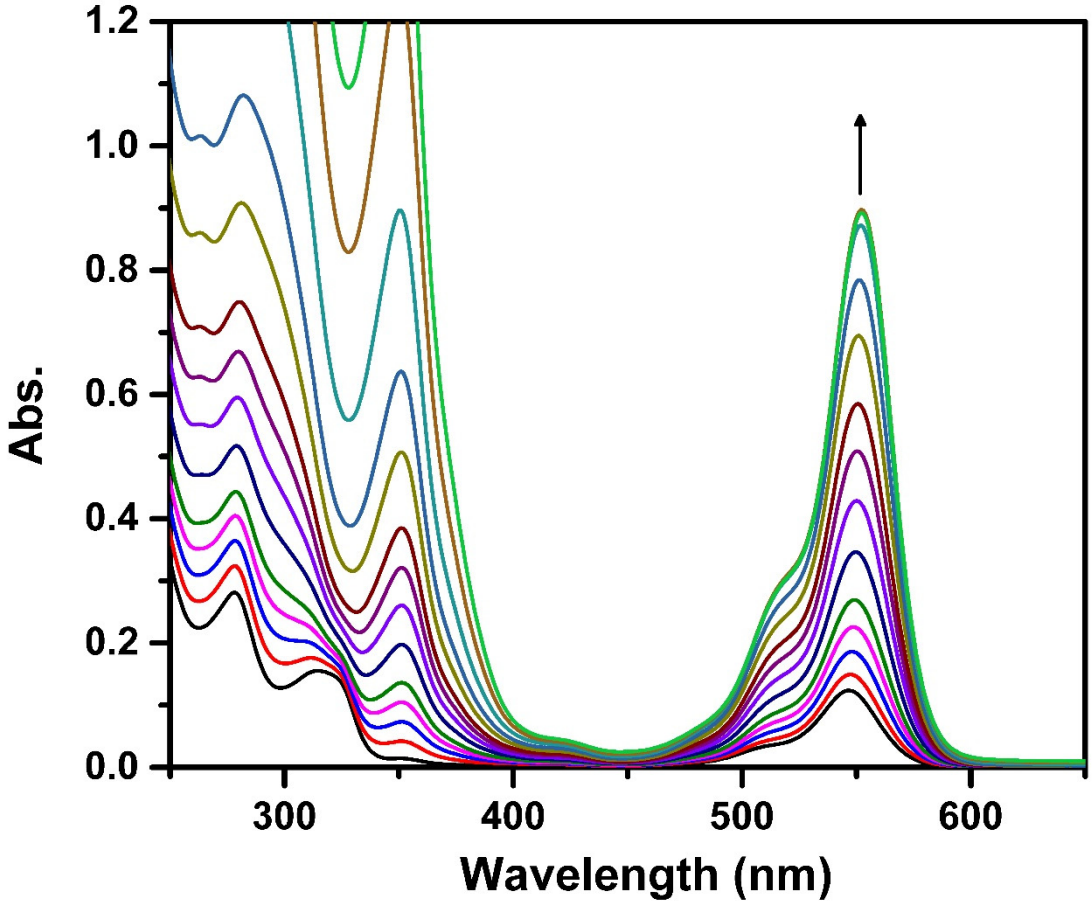

Figure S34. UV-vis absorption curves of Rhodamine B base titrated with **2-Co**. The arrow indicates the gradual increase of **2-Co** equivalents.

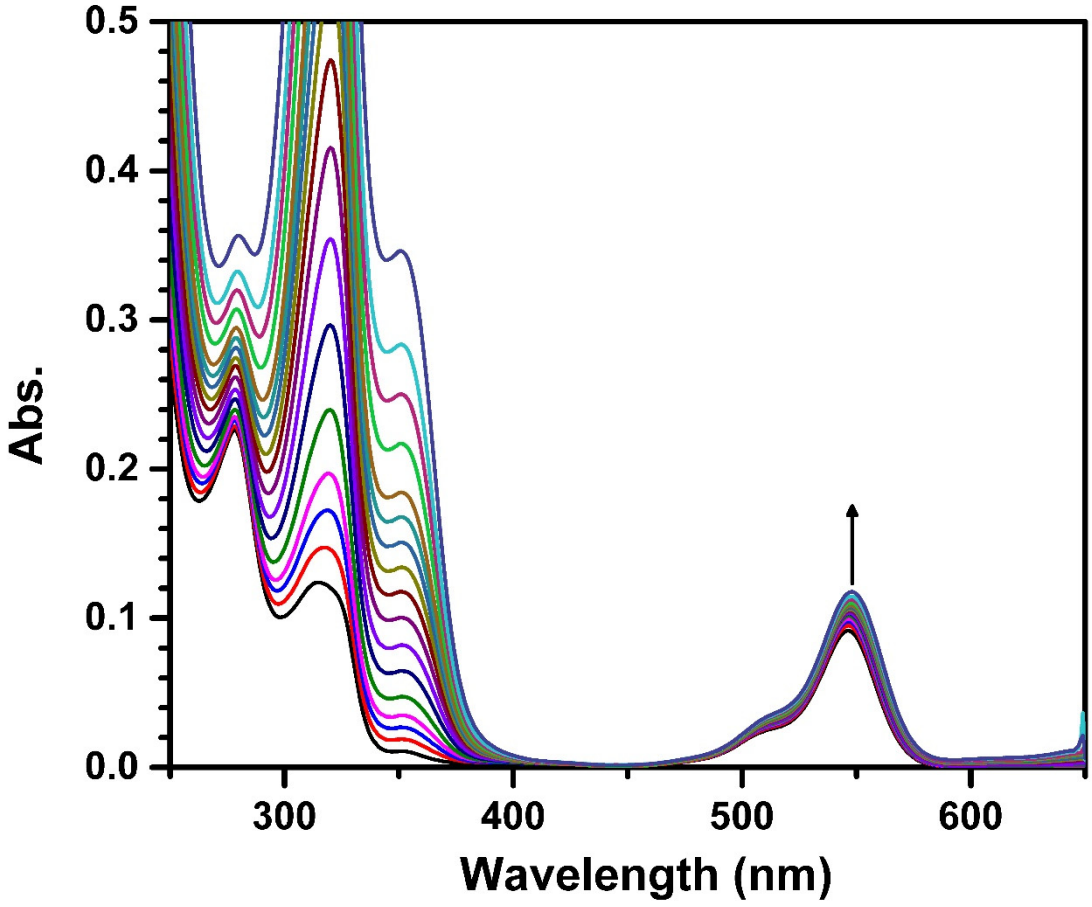

Figure S35. UV-vis absorption curves of Rhodamine B base titrated with *p-tert*-butylsulfonyl-calix[4]arene (TBSC). The arrow indicates the gradual increase of TBSC equivalents.

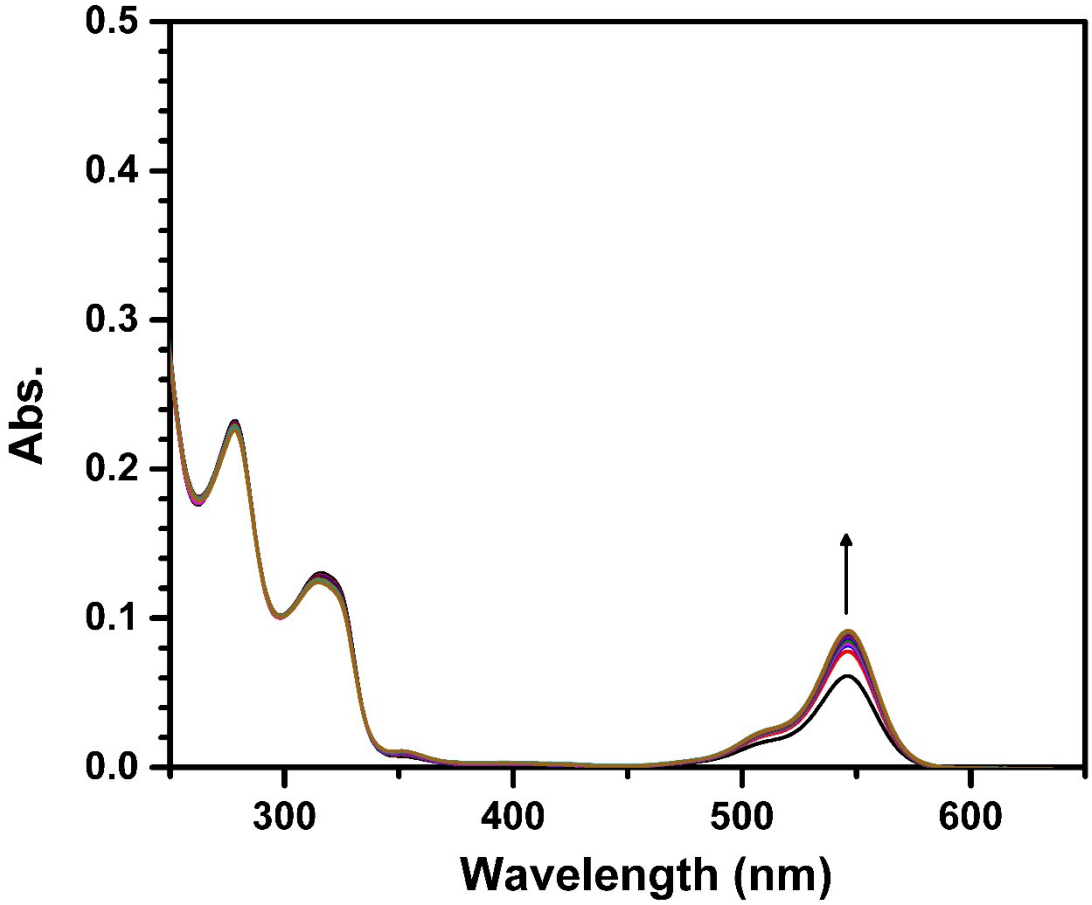

Figure S36. UV-vis absorption curves of Rhodamine B base titrated with $CHCl_3$. The arrow indicates the gradual increase of the amount of $CHCl_3$.

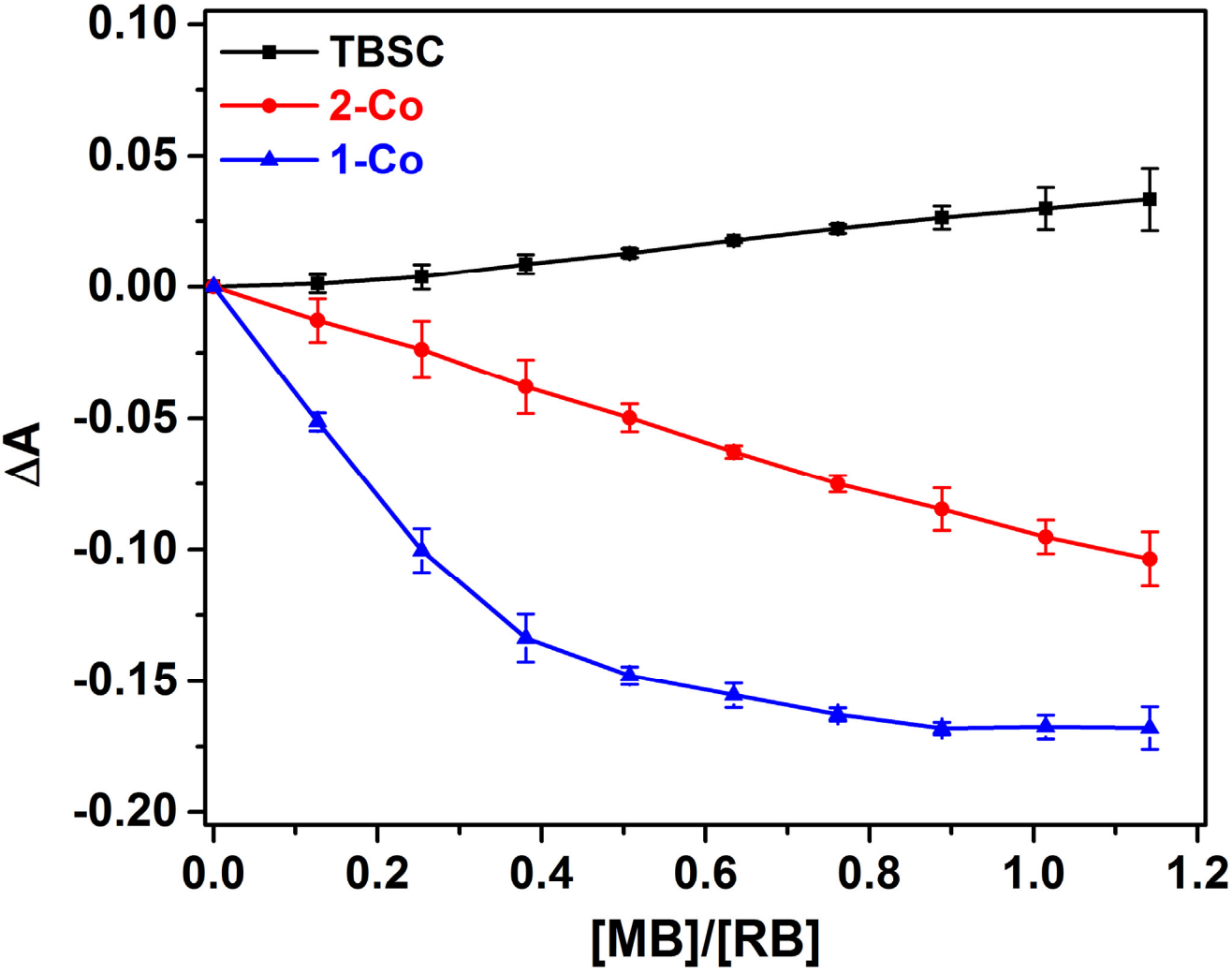

Figure S37. Change of UV-vis absorbance of the RB form in $CHCl_3$ upon titrating MB to the solution. The initial RB solution was in equilibrium with **1-Co**, **2-Co**, or TBSC in a 3:1 molar ratio. The decrease in absorbance for the **1-Co** and **2-Co** solutions indicates that the ring-opened cationic RB form was partially converted to the ring-closed neutral form upon the addition of MB.

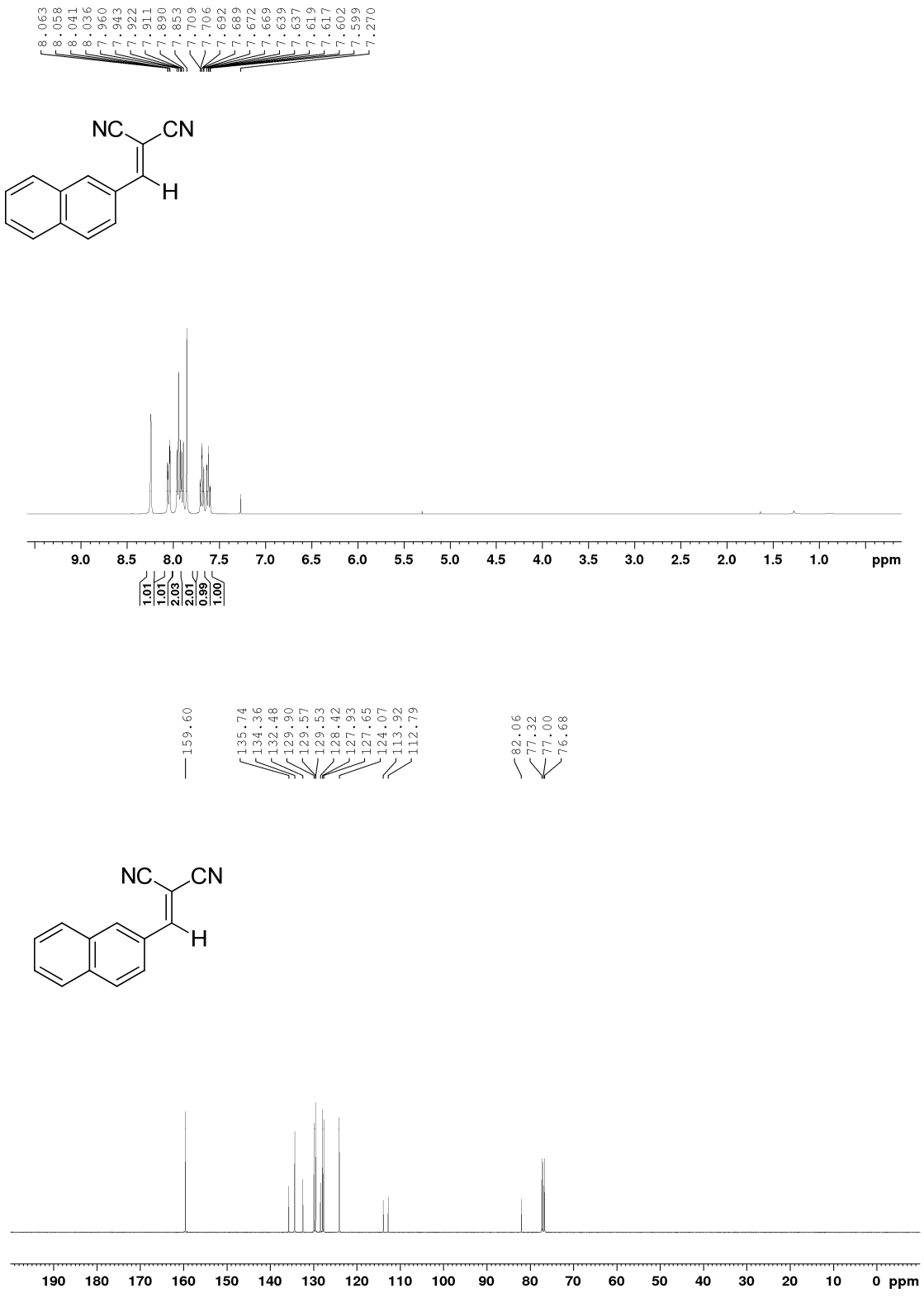

Figure S38. ^{1}H (top) and ^{13}C (bottom) NMR spectra of the Knoevenagel condensation product.

S1. (a) N. Iki, H. Kumagai, N. Morohashi, K. Ejima, M. Hasegawa, S. Miyanari, S. Miyano, *Tetrahedron Lett.* **1998**, *39*, 7559; (b) N. Morohashi, N. Iki, A. Sugawara, S. Miyano, *Tetrahedron*, **2001**, *57*, 5557.

S2. (a) H. Kumagai, M. Hasegawa, S. Miyanari, Y. Sugawa, Y. Sato, T. Hori, S. Ueda, H. Kamiyama, S. Miyano, *Tetrahedron Lett.* **1997**, *38*, 3971; (b) N. Iki, C. Kabuto, T. Fukushima, H. Kumagai, H. Takeya, S. Miyanari, T. Miyashi, S. Miyano, *Tetrahedron*, **2000**, *56*, 1437.

S3. Y.-Y. Liu, Z.-H. Wang, J. Yang, Bo Liu, Y.-Y. Liu and J.-F. Ma, *CrystEngComm*, **2011**, *13*, 3811.

S4. SAINT V6.1, Bruker Analytical X-ray Systems, Madison, WI, **1999**.

S5. G. M. Sheldrick, *SADABS*, Empirical Absorption Correction Program, University of Göttingen, Göttingen, Germany, **1997**.

S6. SHELX97 - Programs for Crystal Structure Analysis (Release 97-2). G. M. Sheldrick, Institüt für Anorganische Chemie der Universität, Tammanstrasse 4, D-3400 Göttingen, Germany, **1998**.

S7. (a) A. L. Spek, *J. Appl. Cryst.* **2003**, *36*, 7-13; (b) A. L. Spek, *Acta Cryst.* **2009**, *D65*, 148.

S8. Schalley, C. A. *Analytical Methods in Supramolecular Chemistry*; Wiley, 2012.

S9. Benesi, H. A.; Hildebrand, J. *J. Am. Chem. Soc.* **1949**, *71*, 2703.

S10. Wiles, C.; Watts, P.; Haswell, S. J. *Lab Chip* **2007**, *7*, 322-330.